



Local ordering and dynamics in anisotropic media by magnetic resonance: from liquid crystals to proteins

Eva Meirovitch & Jack H. Freed

To cite this article: Eva Meirovitch & Jack H. Freed (2020) Local ordering and dynamics in anisotropic media by magnetic resonance: from liquid crystals to proteins, *Liquid Crystals*, 47:13, 1926-1954, DOI: [10.1080/02678292.2019.1622158](https://doi.org/10.1080/02678292.2019.1622158)

To link to this article: <https://doi.org/10.1080/02678292.2019.1622158>



Published online: 01 Jul 2019.



Submit your article to this journal [↗](#)



Article views: 86



View related articles [↗](#)



View Crossmark data [↗](#)



Citing articles: 1 View citing articles [↗](#)

INVITED ARTICLE



Local ordering and dynamics in anisotropic media by magnetic resonance: from liquid crystals to proteins

Eva Meirovitch ^a and Jack H. Freed ^b

^aThe Mina and Everard Goodman Faculty of Life Sciences, Bar-Ilan University, Ramat-Gan, Israel; ^bBaker Laboratory of Chemistry and Chemical Biology, Cornell University, Ithaca, NY, USA

ABSTRACT

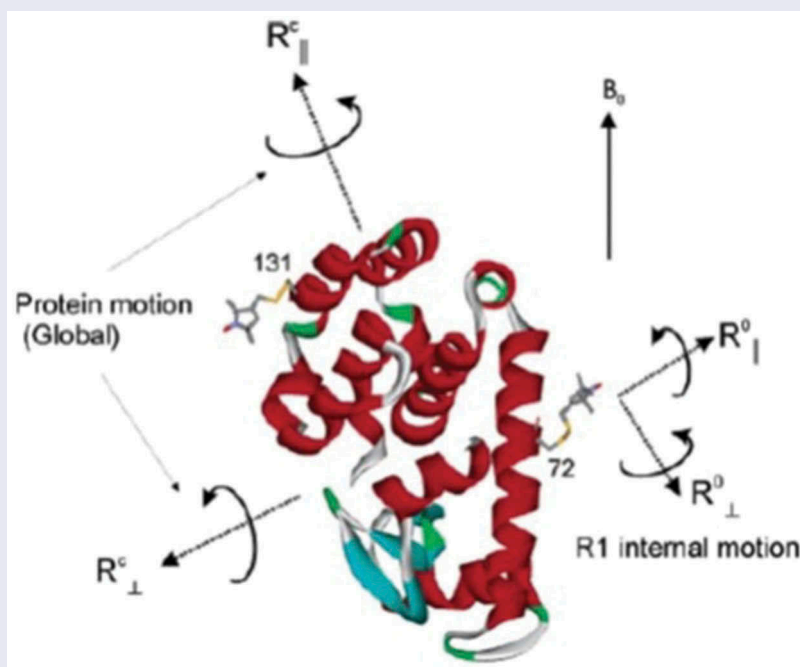
Magnetic resonance methods have been used extensively for over 50 years to elucidate molecular structure and dynamics of liquid crystals (LCs), providing information quite unique in its rigour and extent. The ESR- or NMR-active probe is often a solute molecule reporting on characteristics associated with the surrounding (LC) medium, which exerts the spatial restrictions on the probe. The theoretical approaches developed for LCs are applicable to anisotropic media in general. Of particular interest is the interior space of a globular protein labelled, e.g. with a nitroxide moiety or a ^{15}N - ^1H bond. The ESR or NMR label plays the role of the probe and the internal protein surroundings the role of the anisotropic medium. A general feature of the restricted motions is the local ordering, i.e. the nature, magnitude and symmetry of the spatial restraints exerted at the site of the moving probe. This property is the main theme of the present review article. We outline its treatment in our work from both the theoretical and the experimental points of view, highlighting the new physical insights gained. Our illustrations include studies on thermotropic (nematic and smectic) and lyotropic liquid crystals formed by phospholipids, in addition to studies of proteins.

ARTICLE HISTORY

Received 26 March 2019

KEYWORDS

Anisotropic media; local ordering; stochastic liouville equation; slowly relaxing local structure; microscopic-order-macroscopic-disorder



Introduction

In characterising the dynamic structure of anisotropic media one has to consider the key aspects of restricted motions [1–5]. They include features of ordering,

motion and geometry. The objective is to set forth models for interpreting the relevant experimental data in terms of these properties. We refer here to cases where ESR or NMR probes provide the experimental data that comprise the required information. The

dynamic timescale, determined by the anisotropic magnetic interaction(s), Δ , extends from the rigid-limit (motional rates much smaller than Δ), through the slow-motional regime (motional rates comparable to Δ), all the way to the motional-narrowing regime (motional rates considerably greater than Δ). NMR spectra from molecules in solution are invariably in the motional-narrowing regime as the overall tumbling rates are much larger than Δ ; the slow-motional regime is accessible in the solid state where the overall tumbling is quenched. ESR spectra might cover the entire dynamic range also in solution [3,6].

Several relatively simple models for analysing restricted motions with ESR and NMR methods have been developed over the years; examples can be found in Reference [7] for ESR and in Reference [8] for NMR. In many cases, only the motional-narrowing limit, where the theoretical treatment is simpler but limited in dynamic information, has been considered. Relatively simple stochastic models applicable to the slow-motional regime, adapted to specific situations, have also been developed [9,10]. In such cases several independent simple motional modes had to be combined to reproduce the experimental data; we call such collections multi-simple-mode (MSM) models [8]. Comparison amongst different MSMs is difficult because of mode and model diversity. Improvement requires adding to the collection yet another independent motional mode, changing the overall character while requiring the assumption of mode-independence [8].

Various types of anisotropic media including thermotropic, lyotropic, metallotropic and polymeric liquid crystals (LCs), stretched gels, tobacco mosaic virus assemblies, and certain clays have been studied in the last 50 years [1–5]. More recently, the restricting interior space of proteins or DNA fragments, housing mobile (ESR or NMR) spin-labelled moieties, has been added to the list [7,8]. To better understand the physical basis of restricted motions, it is important to develop methods that can treat a large number of situations and systems in a consistent manner.

Such approaches, applicable over the entire dynamic range, have been developed by Freed and co-workers on the basis of the Stochastic Liouville Equation (SLE) [11–13]. The various physical quantities are represented with due consideration of their three-dimensional tensorial requirements. Rotational motion is represented by a 3D diffusion tensor; orientations between magnetic and molecular tensor frames, and the lab frame, are described by respective Euler angles; and the local ordering is represented by a potential expanded in the basis set of the real linear combinations of the Wigner rotation matrix elements, $D_{M,|K|}^L$

[12,13]. Powerful and effective methods for solving the SLE, notably the Lanczos algorithm, have been developed for the calculation of slow-motional ESR spectra [14–16]. Procedures for determining optimal basis-sets have been provided [17]. Powerful methods for the analysis of the magnetic resonance spectra based on optimised non-linear least-squares (NLLS) algorithms have been developed [18].

These theoretical-computational tools, and typical applications to liquid crystals, have been compiled in References [6,19–22]. Observations of interest were reported in the early work. For example, deviation from Brownian motion of spin-probes was detected in nematic LCs, prompting further theoretical developments [6,19,20]. Likewise, long-range cooperative motions prevailing near phase-transitions, providing insights into thermodynamic properties of the LC medium, were found and analysed [21]. Multi-frequency ESR, covering the 9–250 GHz range, was established following the development of high-frequency ESR spectrometers [23,24]. 2D Fourier-transform ESR techniques, notably 2D Electron-Electron Double Resonance (ELDOR) [25–28], were developed in the Freed laboratory. Reference [29] is a comprehensive compendium which summarised these advances in 1989. The technique of 2D-ELDOR substantially broadens the scope of the ESR investigations of structure and dynamics, and the elucidation of features of local ordering and dynamics in particular.

The nematic director (direction of preferred orientation) usually orients parallel to the external magnetic field, B_0 , of the ESR or NMR spectrometer. In the smectic phase this director, usually frozen in direction, can be tilted relative to B_0 [2,3,13,20]. This provides an orientation-dependence which is a useful feature; however, this symmetry-breaking tilt required developing appropriate theoretical-computational tools to be able to analyse such spectra in the sensitive slow-motional regime. The SLE implemented in Reference [16] meets this challenge. The Standard Liquid Crystal (SLC) methodology was extended to the case where the LC (or nematic) director is distributed in space at random, yielding the microscopic-order-macroscopic-disorder (MOMD) model [30]. The MOMD model applies, for example, to dispersions of nitroxide-doped artificial [30–32] and biological [33,34] membranes. In these cases, MOMD describes the motion as a composite of the various component motions, both internal and overall [35]. In the limiting case where the overall motion is slow enough to appear frozen out, MOMD just reflects the faster internal motion. MOMD also has been applied to nitroxide-labelled internally mobile

proteins in solution [36] and to NMR-labelled polycrystalline powders of internally mobile proteins [8,37–40].

Freed et al. developed a model which does differentiate and characterise the usually slower overall motions and the faster local motions [41,42]. The overall motion may be unrestricted (as in aqueous solutions of internally mobile nitroxide-labelled proteins [36,43], DNA fragments [44], or NMR-labelled proteins [45–48]) or restricted (as for probes reorienting in thermotropic or lyotropic LC media, or membrane proteins reorienting in lipid bilayers) [35]. The overall motion is invariably restricted by the local ‘cage’ in anisotropic fluids [49,50], and the local motion by the immediate (internal) surroundings in internally mobile molecules.

These local and overall motions are coupled dynamically, with the local motion being typically faster than the overall motion, i.e. the local motion occurs within the frame of the overall tumbling motion. The dynamical coupling materialises in the theory through a potential; from the perspective of the probe, this is an ordering potential. This theory is a many-body stochastic approach to rotational motions in liquids [41,42]. Its two-body version is the slowly relaxing local structure (SRLS) model: body 1 is the macromolecule/lipid, and body 2 is the probe. Dynamical coupling is a fundamental property present even in simple limits – cf. the perturbational expansions of SRLS developed in early work [13,51], where body 1 is a slowly reorienting solvent ‘cage’ and body 2 is a probe reorienting rapidly inside that ‘cage’.

In addition to its application to the analysis of continuous-wave (CW) ESR lineshapes, the SRLS approach was also applied to the analysis of 2D-ELDOR lineshapes [49,50]. The more recent development of SRLS to NMR relaxation in proteins is described in References 45–48.

Following a brief summary of the theoretical background, we show representative examples of the key role played, and the information provided, by the local ordering as determined with the SLC, MOMD and SRLS models. As already noted, the local ordering is expressed in terms of a (dimensionless) local potential, u , expanded in the basis set of the real linear combinations of the Wigner rotation matrix elements, $D_{0|K|}^L$, $L = 1 \dots \infty$, $|K| = 0, \dots, L$. In the case of most thermotropic liquid crystals, symmetry requires only values of even L , although in lipid membranes, proteins, and other systems of polar character, odd L values should be significant. For convenience typically only the $L = 2$, $|K| = 0, 2$ terms, with coefficients c_0^2 and c_2^2 , have been kept. In

some cases, the $L = 4$, $|K| = 0, 2$ terms [42], as well as the odd L values of 1 and 3 [52], have been included in the expression for u . Even the potential comprising only the $L = 2$, $|K| = 0, 2$ terms is substantially more general than the potentials used by other authors [9,10]. Importantly, its form is determined within the scope of a physically well-conceived theoretical formulation. Order parameters, S_0^2 and S_2^2 , which are the principal values of the second-rank traceless irreducible ordering tensor, \mathbf{S} , may be defined in terms of c_0^2 and c_2^2 . That is, the local ordering is characterised by a potential, u , and an ordering tensor, \mathbf{S} . With u in hand one can calculate the probability distribution, $P_{\text{eq}} = \exp(-u)/Z$ (Z – partition function), and subsequently any ensemble average (in addition to order parameters), e.g. entropy.

Theoretical summary

Smoluchowski equation for rotational reorientation

This equation is given by [20]:

$$\frac{\partial P_R(\Omega, t)}{\partial t} = \left\{ \mathbf{J} \cdot \mathbf{R}_R(\Omega) \cdot \left[\mathbf{J} + \left(\mathbf{J} \frac{U_R(\Omega)}{kT} \right) \right] \right\}, \quad (1)$$

where $P_R(\Omega, t)$ (the subscript, R, stands for ‘rotation’) is the time-dependent probability distribution for the orientation of a molecule (specified by the set of Euler angles $\Omega(\alpha, \beta, \gamma)$) relative to a laboratory-fixed coordinate frame. $\mathbf{R}_R(\Omega)$ is the diffusion tensor for rotational reorientation assumed to be time-independent in the molecular frame, \mathbf{J} is the vector operator for infinitesimal rotation, and $U_R(\Omega)$ is the ordering potential.

For an axially symmetric diffusion tensor and $U_R(\Omega) = 0$ one has:

$$\mathbf{J} \cdot \mathbf{R}_R(\Omega) \cdot \mathbf{J} = - \left[R_{R,\perp} \mathbf{J}^2 + (R_{R,\parallel} - R_{R,\perp}) (\hat{\mathbf{J}}_z)^2 \right], \quad (2)$$

where $R_{R,\parallel}$ and $R_{R,\perp}$ are the principal values of the diffusion tensor, $\mathbf{R}_R(\Omega)$.

The explicit general forms of the operators \mathbf{J}^2 and \mathbf{J}_z are [20]:

$$\mathbf{J}^2 = - \left[\frac{\partial^2}{\partial \beta^2} + \cot \beta \frac{\partial}{\partial \beta} + \frac{1}{\sin^2 \beta} \left(\frac{\partial^2}{\partial \alpha^2} + \frac{\partial^2}{\partial \gamma^2} \right) - 2 \frac{\cos \beta}{\sin^2 \beta} \frac{\partial^2}{\partial \alpha \partial \gamma} \right] \quad (3)$$

and

$$\mathbf{J}_z = -i \frac{\partial}{\partial \gamma} \quad (4)$$

$U_R(\Omega)$ in Equation (1) is the Potential of Mean Torque (POMT). The actual torque exerted in the equilibrium fluid on the molecule with orientation, Ω , is:

$$\mathbf{T}(\Omega) = i\mathbf{J}U_R(\Omega). \quad (5)$$

The precise definition of the operator, \mathbf{J} , is [12]:

$$\begin{aligned} \mathbf{J}^2 \Phi_{KM}^L(\Omega) &= L(L+1) \Phi_{KM}^L(\Omega) \\ \mathbf{J}_{\pm} \Phi_{KM}^L(\Omega) &= [(L \mp K)(L \pm K + 1)]^{1/2} \Phi_{(K \pm 1)M}^L(\Omega) \\ \mathbf{J}_z \Phi_{KM}^L(\Omega) &= K \Phi_{KM}^L(\Omega), \end{aligned} \quad (6)$$

where the eigenfunctions, $\Phi_{KM}^L(\Omega)$, and the operators, \mathbf{J}_{\pm} , are given by:

$$\Phi_{KM}^L(\Omega) = \left[\frac{(2L+1)}{8\pi^2} \right]^{1/2} D_{MK}^L(\Omega) \quad (7)$$

$$\mathbf{J}_{\pm} \equiv \mathbf{J}_x \pm i\mathbf{J}_y. \quad (8)$$

\mathbf{J}_x , \mathbf{J}_y and \mathbf{J}_z are the components of the operator, \mathbf{J} , in the Principal Axes System (PAS) (call it M frame) of the ordering tensor, \mathbf{S} . For simplicity, this PAS is taken the same as that of the diffusion tensor, $\mathbf{R}_R(\Omega)$.

The equilibrium solution of Equation (1) is given by:

$$P(\Omega) = \exp[-U_R(\Omega)/kT]/Z, \quad (9)$$

Accounting for the fact that the potential has to be real, Equation (1) may be recast as:

$$\frac{\partial P_R(\Omega, t)}{\partial t} = -\Gamma_R(\Omega)P_R(\Omega, t). \quad (10)$$

Following the symmetrisation operation ($\tilde{\Gamma} = P^{-1/2} \Gamma P^{1/2}$ and $\tilde{P} = P^{-1/2} P$) one obtains [20]:

$$\tilde{\Gamma}_{\Omega} = \mathbf{J} \cdot \mathbf{R}_R \cdot \mathbf{J} + \frac{(\mathbf{J} \cdot \mathbf{R}_R \cdot \mathbf{J}U)}{2kT} + \frac{(\mathbf{T} \cdot \mathbf{R}_R \cdot \mathbf{T})}{(2kT)^2} \quad (11)$$

$$\tilde{\Gamma}_{\Omega} = \Gamma_{\text{iso}} + \Gamma_U \quad (12)$$

where

$$\Gamma_{\text{iso}} = \mathbf{J} \cdot \mathbf{R}_R(\Omega) \cdot \mathbf{J} = -[R_{R,\perp} \mathbf{J}^2 + (R_{R,\parallel} - R_{R,\perp}) \mathbf{J}_z] \quad (13)$$

and

$$\begin{aligned} \Gamma_U &= (2kT)^{-1} [R_{R,\perp} (\mathbf{J}^2 U) + (R_{R,\parallel} - R_{R,\perp}) (\mathbf{J}_z^2 U)] \\ &\quad - (2kT)^{-2} [R_{R,\perp} (\mathbf{J}_+ U) (\mathbf{J}_- U) + R_{R,\parallel} (\mathbf{J}_z U)^2]. \end{aligned} \quad (14)$$

Translational diffusion will not be considered here, but see Reference [19]. For convenience, we omit below the subscript, R.

Uniaxial media: potentials, $U(\Omega)$, and associated order parameters

In uniaxial media, only the Wigner rotation matrix elements with $M = 0$, i.e. $D_{0K}^L(\beta, \gamma)$, survive in the expansion of $U(\Omega)$. One has $U(\beta, \gamma)$, where β and γ are the angles defining the orientation of the local ordering frame, M, in the director frame, C [12]. Let us consider an oriented (monodomain) nematic phase where the laboratory frame, L, and the director frame, C, are parallel to the external magnetic field, B_0 . The corresponding SLE frame scheme is depicted in Figure 1.

For uniaxial media that exhibit inversion symmetry with respect to the origin of the C frame (e.g. non-polar LCs), only even- L terms survive. We refer below to such cases, unless otherwise specified. One has [12]:

$$U(\beta, \gamma) = - \sum_{L,K} c_{0K}^L D_{0K}^L(\beta, \gamma) \quad (15)$$

The dimensionless potential for $L = 2$, $|K| = 0, 2$ is given by:

$$u(\beta, \gamma) \equiv U(\beta, \gamma)/kT = -c_0^2 D_{00}^2(\beta, \gamma) - c_2^2 (D_{02}^2(\beta, \gamma) + D_{0-2}^2(\beta, \gamma)). \quad (16)$$

In irreducible tensor notation, one may define five order parameters in terms of the potential of Equation (16). They are given by [7,12]:

$$\begin{aligned} D_{0K}^2(\beta, \gamma) &= \left\{ \int \sin \beta d\beta d\gamma D_{0K}^2(\beta, \gamma) \exp[-u(\beta, \gamma)] \right\} \\ &\quad / \int \sin \beta d\beta d\gamma \exp[-u(\beta, \gamma)] \end{aligned} \quad (17)$$

where $K = -2, \dots, 2$. For at least three-fold (C_{3v} point-group) symmetry around the local director, C,

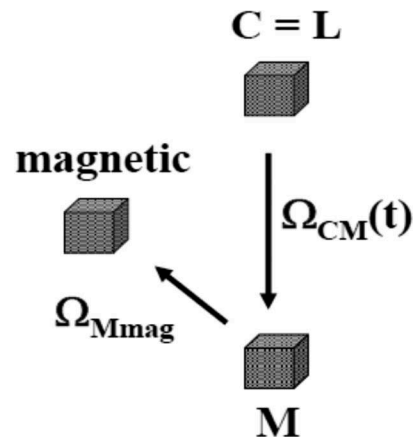


Figure 1. SLE frame scheme for L (laboratory frame), B_0 (external magnetic field direction) and C (director frame) being the same. M – local ordering/local diffusion frame; ‘magnetic’ – NMR interaction frame (if several magnetic interactions enter the analysis, the designation ‘magnetic’ will include the corresponding magnetic frames). The Euler angles Ω_{CM} are time-dependent; the Euler angles Ω_{Mmag} are time-independent.

and at least two-fold symmetry (D_{2h} point-group) around Z_M , only $S_0^2 = \langle D_{00}^2(\beta, \gamma) \rangle$ and $S_2^2 = \langle D_{02}^2(\beta, \gamma) + D_{0-2}^2(\beta, \gamma) \rangle$ survive in the M frame. The principal values of S tensor in Saupe-tensor notation, S_{xx} , S_{yy} and S_{zz} , relate to S_0^2 and S_2^2 as $S_{xx} = (\sqrt{3/2}S_2^2 - S_0^2)/2$, $S_{yy} = -(\sqrt{3/2}S_2^2 + S_0^2)/2$ and $S_{zz} = S_0^2$. [2,3,20] If three-fold symmetry also prevails around Z_M , the coefficient c_2^2 in Equation (16) will be zero, and $S_2^2 = 0$. The order parameters associated with $L \neq 2$ are defined by analogy, assuming that they are diagonal in the PAS of the second-rank ordering tensor.

The constituents of $u(\beta, \gamma)$ are real combinations of the $D_{0K}^L(\beta, \gamma)$ functions, which belong to the D_{2h} point group [53]. Thus, it seems reasonable to impose effective D_{2h} point group symmetry on $u(\beta, \gamma)$ (note also that D_{2h} point group symmetry is inherent to the definition of the diffusion tensor, R , whose PAS is taken here the same as that of the ordering tensor, S , defined in terms of $u(\beta, \gamma)$).

Other symmetries of the local potential

Monodomain nematic and smectic A LCs exhibit inversion symmetry with respect to the origin of the director frame. In a simple sense, the ordering of a large solute probe reorienting in such an LC may be taken as reflecting this inversion symmetry. This scenario represents ‘non-polar’ ordering; consequently, the local potential comprises only even- L terms (e.g. see Reference [52]). The ordering may be thought of as a preferential arrangement in space of double-headed-arrows, a setup often referred to as *alignment* [1,54]. The leading terms here are the real linear combination of the functions D_{0K}^2 with $L = 2$, $|K| = 0, 1, 2$ (more generally, $L = 2, 4, 6 \dots$).

Envision a smaller probe residing, e.g. in one leaflet of a lipid bilayer. The local environment is most certainly polar, requiring odd- L terms to be retained in the expression of the potential. This type of ordering, associated with a uniaxial polar director, may be thought of as preferential arrangement in space of single-headed arrows, which is often referred to as *orientation* [1,54].

Now consider a probe which is a spin-labelled structural moiety reorienting in the anisotropic inner space of a protein. The fact that the probe is attached physically to the protein implies a single-headed-arrow-type, i.e. polar, ordering. As indicated above, this scenario is represented by taking the local director to be uniaxial and polar. The local potential should feature odd- L terms, the leading ones being the real linear

combinations of the functions D_{0K}^L with $L = 1, |K| = 0, 1$ (more generally, $L = 1, 3, 5 \dots$).

The D_{2h} point group comprises non-polar/‘gerade’ (labelled ‘g’) and polar/‘ungerade’ (labelled ‘u’) irreducible representations (see Character Table of the D_{2h} point group given in [Table 1]);[52]. The potentials, $u(\beta, \gamma)$, may thus be characterised on the basis of the irreducible representations of the D_{2h} point group. The polar constituents/terms with odd- L correspond to the irreducible representations A_u, B_{1u}, B_{2u} or B_{3u} , whereas the non-polar constituents with even- L correspond to the irreducible representations A_g, B_{1g}, B_{2g} or B_{3g} . This is an interesting new perspective for characterizing local ordering in proteins. In view of the various approximations, admixtures are probably realistic (see below).

Biaxial media are discussed in Reference [19]; here we forgo considering such media in detail, except for pointing out the observation of local biaxiality in oriented phospholipid bilayers studied at 250 GHz microwave frequency [55].

Director tilt

As pointed out above, the SLE of Freed et al. is applicable to slow-motional ESR spectra wherein the LC directors are tilted with respect to the external field, B_0 [16]. The corresponding frame scheme is depicted in Figure 2. The time-independent Euler angles Ω_{LC} represent the director tilt. For uniaxial C (L is inherently uniaxial), only the polar angle, β_{LC} survives. Note that $\Omega_{CM} = -\Omega_{LC} + \Omega_{LM}$. In this notation the Ω_{LM} is

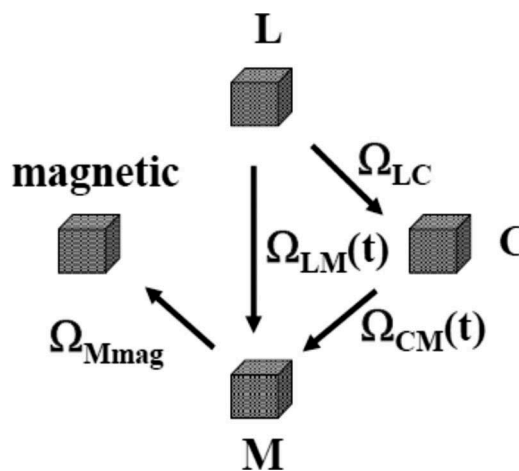


Figure 2. SLE frame scheme for liquid-crystal director (C frame) tilted with respect to the external magnetic field, B_0 (L frame); the Euler angles Ω_{LC} are time-independent. The M and ‘magnetic’ frames, and the Euler angles Ω_{CM} and Ω_{Mmag} – as in the captions of Figure 1.

applied first and then the $-\Omega_{LC}$ is applied. As is well known, these 3D rotations do not commute.

Now assume that the Euler angles, Ω_{LC} , are distributed in space at random; this is the MOMD model [30]. One has to calculate ESR or NMR spectra for a sufficiently large number of Ω_{LC} values and superpose the respective lineshapes to obtain the MOMD spectrum [30].

Additional aspects

Fluctuations in the local structure (the simple limit of the SRLS model) are discussed in Reference [19]. Magnetic parameters, effective Hamiltonian, spectral densities and linewidths are discussed for nitroxides in Reference [20]. Of interest in the present context are the order parameters S_0^2 and S_2^2 . The conditions under which these quantities can be derived directly from the experimental spectra are specified in Reference [20]. In general, all of the physical parameters associated with ordering, motion and geometry are obtained by fitting sets of ESR spectra acquired at various temperatures, and/or pressures, and/or microwave frequencies [18]. The ESR spectra may be of the 1D CW or 2D-ELDOR type.

The stochastic Liouville equation (SLE)

We refer to the SLE for a probe reorienting in an anisotropic medium with director C (frame scheme shown in Figure 2 with Ω_{LC} fixed). The coordinates Ω_o characterise the orientation of the probe with respect to the laboratory frame. The ESR spin Hamiltonian describing the magnetic interactions associated with a nitroxide radical is given by [42]:

$$\hat{\mathcal{H}} = (\beta_e/\hbar)\mathbf{B}_0 \cdot \mathbf{g} \cdot \hat{\mathbf{S}} + \gamma_e \hat{\mathbf{I}} \cdot \mathbf{A} \cdot \hat{\mathbf{S}}, \quad (18)$$

where β_e is the Bohr magneton, \hbar the Planck constant, γ_e the electron gyromagnetic ratio, and the Hamiltonian is expressed in angular frequency units. The first term is the electron Zeeman interaction with \mathbf{B}_0 . The second term describes the hyperfine interaction between the nuclear spin operator, $\hat{\mathbf{I}}$, and the electron spin operator, $\hat{\mathbf{S}}$. The \mathbf{g} and \mathbf{A} tensors depend on the coordinates Ω_o . The nuclear Zeeman terms for nitrogen nuclei with spin equal to 1 are generally neglected in Equation (18).

According to the stochastic Liouville approach, the evolution in time of the density matrix operator, $\hat{\sigma}(\Omega_o, t)$, which represents the joint evolution of the quantum spin degrees of freedom and the classical

motion coordinates, Ω_o , is described by the semi-classical Stochastic Liouville Equation (SLE) [42]:

$$(\partial/\partial t)\hat{\sigma}(\Omega_o, t) = -(\hat{\Gamma} + i\hat{\mathcal{H}}^x)\hat{\sigma}(\Omega_o, t), \quad (19)$$

where $\hat{\mathcal{H}}^x$ is the quantum Liouville operator, i.e. the commutator superoperator defined with respect to $\hat{\mathcal{H}}$, and $\hat{\Gamma}$ is a Markovian operator which we take to be given by the Smoluchowski operator defined by Equations (12)–(14). The quantity $(\hat{\Gamma} + i\hat{\mathcal{H}}^x)$ is referred to as the stochastic Liouville operator.

The ESR (or NMR, using the appropriate spin-Hamiltonian) spectrum for an unsaturated frequency-swept CW spectrum is given by [42]:

$$I(\omega) = \frac{1}{\pi} \mathcal{R}\langle v | [(\hat{\Gamma} + i\hat{\mathcal{H}}^x) + i(\omega - \omega_0)\hat{\Gamma}]^{-1} | v \rangle, \quad (20)$$

where ω is the sweep frequency, $\omega_0 = g_0 \mathbf{B}_0/\hbar = \gamma_e \mathbf{B}_0$ with $g_0 = 1/3 (g_{xx} + g_{yy} + g_{zz})$ (where (x, y, z), denotes the laboratory frame). The starting vector, $|v\rangle$, with respect to which the resolvent is evaluated, is an operator in Hilbert space acting on the spin degrees of freedom; it is also a function of the probe coordinates, Ω_o . The symbol \mathcal{R} in Equation (20) implies the real part of the expression which it precedes.

The slowly relaxing local structure (SRLS) approach

The stochastic description of Equation (19) includes only simple probe reorientation. This is equivalent to a Brownian-like assumption where the immediate surroundings of the probe produce random forces and torques with a white-noise spectrum. To account for dynamic modes arising from the local behaviour of the immediate surroundings of the probe, the Smoluchowski operator, $\hat{\Gamma}(\Omega_o)$ (Equations (11)–(14)), becomes the augmented Smoluchowski operator, $\hat{\Gamma}(\Omega_o, \Omega_c)$, which includes the dynamic effects associated with the immediate surroundings of the probe in the form of additional degrees of freedom, Ω_c , coupled to the probe degrees of freedom, Ω_o . The SRLS equation is obtained from Equation (19) by replacing $\hat{\sigma}(\Omega_o, t)$ with $\hat{\sigma}(\Omega_o, \Omega_c, t)$ and $\hat{\Gamma}(\Omega_o)$ with $\hat{\Gamma}(\Omega_o, \Omega_c)$. Formally Figure 2, with the Euler angles Ω_{LC} being now time-dependent, applies to the case where the surroundings represent an isotropic external medium so that C represents both the rotational diffusion of the medium and the local director for restricted probe motion [41].

The formulation developed in Reference [42] allows for anisotropic external media. In this case, there are three types of potentials describing the local ordering, all of them taken to comprise the $L = 2$, $|K| = 0, 2$ terms. The local potential on the probe has coefficients

c_0^2 and c_2^2 ; the mean-field potential representing the alignment of the probe in the anisotropic external medium has coefficients a_0^2 and a_2^2 (see below); and the mean-field potential representing the alignment of the ‘cage’ in the external anisotropic medium has coefficients b_0^2 and b_2^2 [42].

SRLS Smoluchowski operator for protein dynamics

We refer to the application of SRLS to an internally mobile nitroxide-ESR-labelled or heteronuclear-NMR-labelled protein tumbling in isotropic solution. In this case, the probe (body 2 or rotator 2) is a rigid spin-labelled moiety reorienting locally in a restricted manner, while its immediate surroundings represented by the protein (body 1 or rotator 1) are tumbling in solution. The frame scheme for this case is shown in Figure 3.

A new frame – C' – appears in Figure 3; it represents the local director frame, typically taken uniaxial. In general, C' is not the same as the global diffusion frame, C , unless the latter is isotropic. For example, taking C to be axial (cigar-shaped protein), the time-independent Euler angles, $\Omega_{CC'}$, are given by $(0, \beta_{CC'}, 0)$, with $\beta_{CC'}$ denoting the tilt angle between the (axial) C and C' frames.

Let us assume for simplicity that C and C' are the same ($\beta_{CC'} = 0$). The SRLS operator is given by [45]:

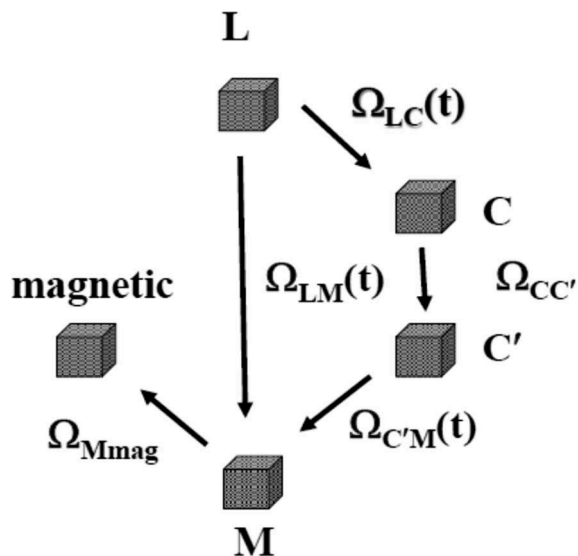


Figure 3. Frame scheme for an internally mobile spin-labelled protein in isotropic solution. L – laboratory frame parallel to B_0 ; C – global diffusion frame; C' – local director frame; M – local ordering/local diffusion frame; ‘magnetic’ refers to the relevant magnetic frame(s). The Euler angles Ω_{LC} (global motion) and $\Omega_{C'M}$ (local motion) are time-dependent; the Euler angles $\Omega_{CC'}$ and Ω_{Mmag} are time-independent.

$$\hat{\Gamma} = \hat{\Gamma}^{\text{global}}(\Omega_{LC}) + \hat{\Gamma}^{\text{local}}(\Omega_{LM}) + F^{\text{global}}(-\Omega_{CM}) + F^{\text{local}}(\Omega_{CM}). \quad (21)$$

The first term of Equation (21) refers to the global-motional rotator and the second term to the local-motional rotator in the absence of a coupling potential. For isotropic global motion one has:

$$\hat{\Gamma}^{\text{global}}(\Omega_{LC}) = R^c(\hat{\mathbf{J}}^c)^2, \quad (22)$$

where $\hat{\mathbf{J}}^c$ is the operator for infinitesimal rotation associated with this motion (cf. Equations (6)). $R^c = 1/(6\tau_c)$ is the diffusion rate constant for global motion.

The local motion term is taken (in the absence of a coupling potential) as an axially symmetric diffusion tensor:

$$\hat{\Gamma}^{\text{local}}(\Omega_{LM}) = R_{\perp}^o(\hat{\mathbf{J}}^o)^2 + (R_{\parallel}^o - R_{\perp}^o)(\hat{\mathbf{J}}_z^o)^2, \quad (23)$$

where $\hat{\mathbf{J}}^o$ is the operator for infinitesimal rotation for this motion, $\hat{\mathbf{J}}_z^o$ is its z -component in the local diffusion frame (cf. Equations (6)), and R_{\parallel}^o and R_{\perp}^o are the principal values of the local diffusion tensor in the M frame.

The motion of the probe in the interior space of the protein is restricted by the potential, $U(\Omega_{CM})$, which couples the global and local motions. The terms F^{global} and F^{local} in Equation (21) represent this coupling. They are functions of the Euler angles $\Omega_{CM} = -\Omega_{LC} + \Omega_{LM}$ which transform the C frame into the M frame (Figure 3). The operator expressions for F^{global} and F^{local} are [45]:

$$F^{\text{local}} = \left(\frac{1}{2}\right) \left[R_{\perp}^o \left((\hat{\mathbf{J}}^o)^2 u \right) + (R_{\parallel}^o - R_{\perp}^o) \left((\hat{\mathbf{J}}_z^o)^2 u \right) - \left(\frac{1}{4}\right) \left[R_{\perp}^o \left(\hat{\mathbf{J}}_+^o u \right) \left(\hat{\mathbf{J}}_-^o u \right) + R_{\parallel}^o \left(\hat{\mathbf{J}}_z^o u \right)^2 \right] \right] \quad (24a)$$

and

$$F^{\text{global}} = \left(\frac{1}{4}\right) R^c \left[(2(\hat{\mathbf{J}}^c)^2 u) - (\hat{\mathbf{J}}_+^c u)(\hat{\mathbf{J}}_-^c u) + (\hat{\mathbf{J}}_z^c u)^2 \right], \quad (24b)$$

where $u \equiv U(\Omega_{CM})/kT$, from which S_0^2 and S_2^2 may be determined (cf. discussion following Equation (17)). The latter are the order parameters.

Local ordering at mobile sites in heteronuclear-NMR-labelled proteins – a feature of particular interest – has been treated traditionally with the model-free (MF) method [56,57]. MF is a simple limit of SRLS without a physically defined potential and with the various tensors having the highest possible symmetry.

Rather than an axial (highest-symmetry) ordering tensor, \mathbf{S} , with principal value S_0^2 , MF chooses to use a squared generalised order parameter, S^2 , arbitrarily defined as [56]:

$$S^2 = \sum_{K=0,\pm 1,\pm 2} |\langle D_{0K}^2 \rangle \langle D_{0-K}^2 \rangle|, \quad (25)$$

where $\langle \dots \rangle$ denotes averaging over the local motion.

S^2 is the same in any coordinate frame. In the PAS of the ordering tensor, \mathbf{S} , one has:

$$\begin{aligned} S^2 &= \langle D_{00}^2(\beta) \rangle^2 + 2\{ \text{Re} \langle D_{02}^2(\beta, \gamma) \rangle \}^2 \\ &= (S_0^2)^2 + 0.5(S_2^2)^2, \end{aligned} \quad (26)$$

given that $S_0^2 \equiv \langle D_{00}^2(\beta, \gamma) \rangle$ and $S_2^2 \equiv 2\{ \text{Re} \langle D_{02}^2(\beta, \gamma) \rangle \}$. In the simple limit where $S_2^2 = 0$ and S_0^2 is very large, $S^2 = (S_0^2)^2$ is a physically well-conceived measure of the total mean-squared amplitude of all internal motions [7]. Otherwise S^2 is a composite given by the sum of an axial term and a rhombic term. In some cases, S^2 is converted into conformational entropy [58], the meaning of which is thus physically vague. In molecular dynamics (MD) studies S^2 is calculated often using Equation (25), which implicitly has the meaning of Equation (26).

Results and discussion

The main experimental variables for studying nitroxides are the temperature and the microwave frequency. Figure 4 shows ESR spectra of the nitroxide 2,2,6,6-tetramethyl-4-piperidone N-oxide (PDT) in toluene acquired at 250 GHz microwave frequency over the

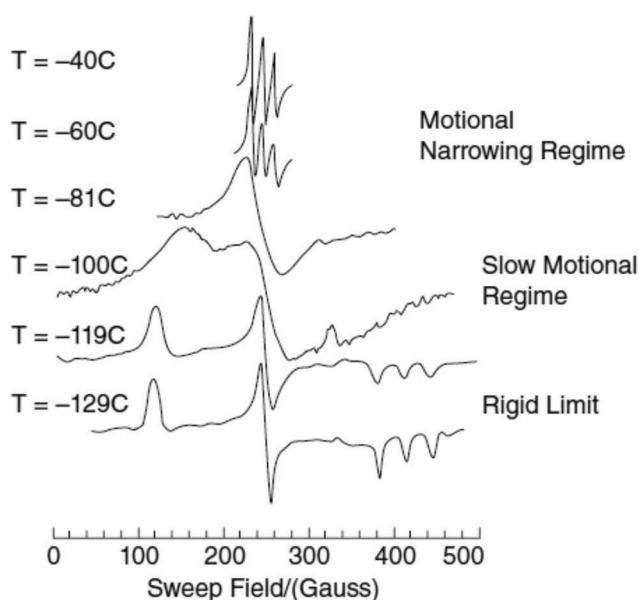


Figure 4. ESR spectra at 250 GHz of PDT in toluene in the -40 to -129°C temperature range [59].

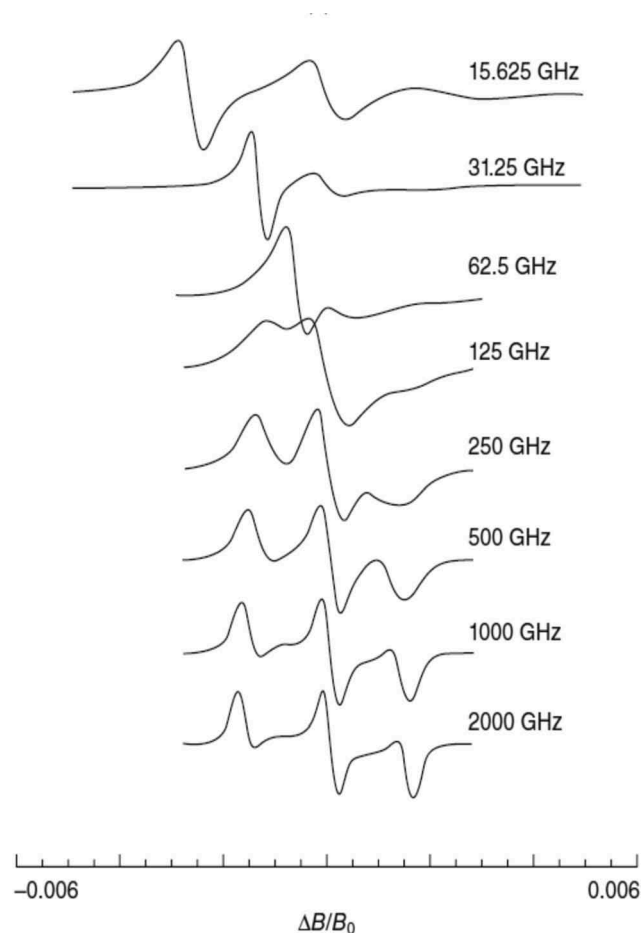


Figure 5. Simulated ESR spectra of a nitroxide reorienting with diffusion rate constant of 10^8 s^{-1} in the microwave frequency range of 15.625–2000 GHz [59].

entire dynamic range [59]. It illustrates the remarkable sensitivity of the slow-motional regime. Figure 5 shows simulated ESR spectra of a nitroxide reorienting with diffusion rate of 10^8 s^{-1} for microwave frequencies spanning the range of 15.635–2000.0 GHz [59]. The ESR lineshapes are also very sensitive to this variable. Among others, Figure 5 illustrates the fact that slow motions affecting the ESR spectrum at low microwave frequencies might be frozen out at high microwave frequencies because of their faster time-scale [23]. As shown below, this is particularly useful for multifrequency ESR applications to proteins in solution. Figures 4 and 5 depict cases with no local ordering; further enhanced sensitivity is featured by ESR spectra in the presence of local ordering.

Local ordering in thermotropic liquid crystals; ESR analysis

Slow-motional ESR analysis of nitroxides dissolved in anisotropic media was first developed in Reference

[11]. In that study, the ordering and diffusion of the probe were taken to be axially symmetric, and the medium was uniaxial with the director parallel to B_0 . Extension to rhombic ordering potentials, and application to PDT dissolved in the liquid crystals butyl-p-(p-ethoxyphenoxy-carbonyl) carbonate (BEPC), p-(p-ethoxyphenyl-azo) phenylhexanoate (PEPH), and p-(N-[p-methoxybenzylideneamino]-n-butylbenzene (MBBA), were first reported in Reference [12]. The motional-narrowing ESR spectra yielded weak rhombic ordering and activation energies characteristic of the twist viscous properties of the liquid crystal. Anomalous behaviour, detected in the incipient slow-motional regime was interpreted in terms of fluctuations in a dynamic slowly relaxing solvent ‘cage’ surrounding the probe, within the scope of a simple treatment.

This anomaly prompted the development of the slowly relaxing local structure model, first formulated in Reference [51] as a perturbational expansion. A slowly moving ‘solvent cage’ houses a rapidly reorienting probe. The two entities are coupled by means of weak fluctuations in the local ‘cage’ structure, expressed as $(S_0^2)^2$. Both the probe and the cage reorient isotropically. The perturbational expansion of SRLS was used within the scope of motional narrowing ESR or NMR, and the magnetic and model tensors were taken diagonal in the same axial frame, for simplicity. The spectral density (obtained by Fourier transformation of the SRLS time-correlation function) is given by [47]:

$$J(\omega) = (S_0^2)^2 \tau_{1,0} / (1 + \omega^2 \tau_{1,0}^2) + \left(1 - (S_0^2)^2\right) \tau_{2,0} / (1 + \omega^2 \tau_{2,0}^2), \quad (27)$$

where 1 stands for ‘cage’, 2 for ‘probe’, and $S_0^2 = \langle D_{00}^2(\Omega_{CM}) \rangle$ is defined in terms of the potential $u = -c_0^2 D_{00}^2$. The term $(S_0^2)^2 \tau_{2,0} / (1 + \omega^2 \tau_{2,0}^2)$ expresses the dynamical coupling between the probe and the ‘cage.’ The spectral density of Equation (27) is formally analogous to the model-free spectral density of Reference [56] but stated and given in the context of liquid crystals 5 years earlier. An enhanced perturbational SRLS expansion suitable for rhombic coupling potential and a 90° tilt between the principal axes of the ordering and magnetic tensors was developed in Reference [13]; the corresponding spectral density is formally analogous to the extended MF spectral density of Reference [57], although presented years earlier.

In Reference [13], the probe PDT, previously used in Reference [12] to study nematics, was used to study the liquid crystals [4'-n-octyl-4-cyanobiphenyl (8CB), N-(p-butoxybenzylidene)-p-n-hexylalinine (4O,6), and N-(p-butoxybenzylidene)-p-n-octylalinine (4O,8)], which exhibit nematic, smectic A and smectic B phases. ESR lineshapes were acquired and analysed as a function of temperature and orientation, θ (β_{LC} in Figure 2), of the director with respect to B_0 . Rhombic ordering was determined in all of the LC phases. In the smectic phases, PDT was found to be gradually expelled from the rigid-core region into the flexible hydrocarbon end-alkyl-chain region of the smectic layer. The temperature-dependent S_0^2 and S_2^2 patterns played a key role in providing new information on the packing of smectic layers. SRLS effects, which impact the local ordering in the flexible end-alkyl-chain region, were detected in the incipient slow-motional regime. Static distortions of the smectic layering introduced by wall-effects, and magnetic-field-induced torques, were also detected.

A method for preparing distortion-free and strongly anchored monodomain smectic LCs between glass surfaces was developed in Reference [60]. The nitroxide N-oxy-4,4-dimethylspiro[oxazolidine-2,3'-5a]-cholestane (CSL) was used to study the benzylidene-type liquid crystals di-heptyloxyazooxybenzene (HOAB), (4O,6) and (4O,8). Motional-narrowing ESR analysis was applied to temperature-dependent and orientation-dependent spectra where appropriate. Slow-motional ESR analysis was applied to spectra where the LC director was parallel to the external magnetic field; for tilted director the slow-motional calculations were too tedious at that time. CSL was found to exhibit axial local ordering, in agreement with its cylindrical symmetry. SRLS-related effects were detected.

In Reference [16] the Lanczos algorithm was implemented in a general and efficient formulation of slow-motional and ordering effects on ESR lineshapes, including tilted directors. Various spin-probes and various LCs were considered. In particular, the nitroxide 2-2'-6-6'-tetramethyl 4-(butyl-oxy)-benzoyl-amino piperidine 1-oxy with perdeuterated piperidine ring (P-probe) was used to investigate the benzylidene-derivative LC 4O,6, the cyanobiphenyl-derivative LC 4-cyano-4'-n-pentyl biphenyl (5CB), and the eutectic mixture of 4-cyano-4'-n-octyl biphenyl, 4-cyano-4'-n-decyl biphenyl and 4-cyano-4'-n-decyl oxy-biphenyl liquid-crystal S2. It was found that the main change upon passing from the nematic to the smectic phase of

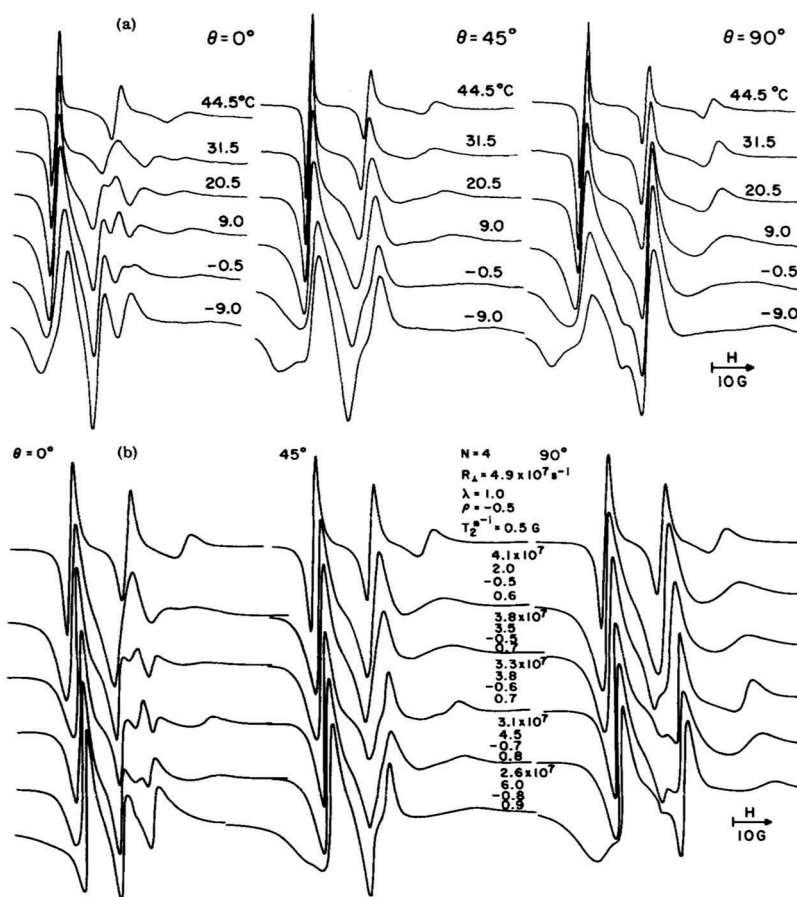


Figure 6. Experimental ESR spectra of the P probe in the smectic A phase of S2 for tilt angles of $\theta = 0^\circ$, 45° and 90° between the LC director and the external magnetic field, B_0 (a). Corresponding calculated ESR spectra with the perpendicular diffusion rate constant, R_\perp the ratio $N = R_\parallel/R_\perp$ the inhomogeneous line-broadening T_2^{*-1} and the potential coefficients λ and ρ depicted. A distribution function reflecting cooperative chain distortions static on the ESR timescale was also included in the calculations of the spectra shown in Figure 6(b) [61].

4O,6 consists of a change in local ordering attributable to packing forces. SRLS effects were detected in 5CB.

The probes CSL and 1,14 stearic acid were used in Reference [61] to study the smectic A phases of 5CB and S2. The analysis of slow-motional orientation-dependent ESR spectra using the effective computer program developed in Reference [16] made possible obtaining detailed information on the local ordering. Figure 6(a) shows temperature-dependent ESR spectra from the smectic A phase of S2 in the (-9) to (44.5) °C range for the director orientations $\theta = 0^\circ$, 45° and 90° . Figure 6(b) shows the corresponding calculated spectra. Out of the various parameters depicted, of interest in the present context are the coefficients λ and ρ of the potential $u(\beta, \gamma) = -\lambda \cos^2\beta - \rho \sin^2\beta \cos 2\gamma$, where λ evaluates the strength of the local potential and ρ its rhombicity (λ and ρ are given in units of kT). This potential represents the recast form of Equation (16) where the free term has been omitted; one has $\lambda = 3/2c_0^2$ and $\rho = \frac{6}{2} c_2^2$ [13].

A relatively weak ordering potential with $\lambda = 1$ at 44.5°C changes gradually to a strong potential with $\lambda = 6$ and at -9°C . The rhombicity of the potential increases with decreasing temperature from $|\rho| = 0.5$ at 44.5°C to $|\rho| = 0.8$ at -9°C , in evidence of more elaborate restraints at lower temperatures attributable to variations in packing forces.

Local ordering in lyotropic liquid crystals; ESR analysis

The slow-motional SLE developed by Freed et al. was also applied to ESR spectra from nitroxides dissolved in lyotropic liquid crystals, in particular phospholipid bilayers. This activity was initiated around 1980 [62]. Since then a large number of phospholipid-bilayer systems in the form of monodomains [63–70] and dispersions [32,33] have been investigated with CW ESR. Phospholipid bilayers in the form of dispersions also have been

investigated with 2D-ELDOR [25–28,71,72]. Features of local ordering have been associated with biological function [33,73–76].

We would like to point out that often order parameters for model and biological membranes are misconstrued as representing ‘membrane fluidity’ [77,78]. Fluidity is a motional parameter whereas ordering is a structural parameter. In SLC, SRS and MOMD there is a clear distinction between structural quantities (potentials and order parameters), dynamical quantities (diffusion rate constants, jump-rates, etc.), geometric quantities (Wigner rotations), and thermodynamic quantities (activation energies). Physically well-conceived membrane fluidity is described, e.g., in Reference [79].

We discuss below representative studies that illustrate the determination of local ordering in model and biological membranes, using SLC, MOMD or SRS analysis of ESR spectra.

Oriented dipalmitoylphosphatidyl choline (DPPC) bilayers with less than 10% water content and 0–4 mol % of the polypeptide gramicidin A (GA) were investigated in Reference [65] with SLC. In the gel phase it was possible to distinguish between two sites – bulk lipid and disordered lipid. It was shown that the latter type is not the usually invoked ‘immobilised lipid’ [77,78], as the diffusion rates are virtually the same for both lipid types. Rather, it is the ordering in the two lipid-types that distinguishes between them. Rhombic ordering was found to prevail in the gel phase, and axial ordering in the LC phase. It was concluded that ‘the principal lipid-GA interaction is that of a boundary effect such that the GA induces disorder in low-temperature and low-water content lipids but it induces order in high-temperature and high-water content (i.e. less ordered) lipids.’ Additional SLE/ESR studies of monodomain membranes are described in References [63,64,66–70].

Utilizing well-resolved monodomain samples is clearly informative. However, often only lipid dispersions are available or relevant. In fact, it was shown in Reference [80] that the lipid structure and dynamics in lipid dispersions and aligned membranes (even when fully hydrated) differ significantly. Lipid dispersions are generally considered a better model for biological membranes. In these cases [31–33,73–76] MOMD [30] applies. Figure 7 illustrates the MOMD analysis: traces two-to-eight correspond to the individual orientations whereas the MOMD spectrum is shown on the top [59].

In recent years, the MOMD model has been utilised to study by ESR the initial stages of the viral attack on membranes, in particular the role of the fusion peptide

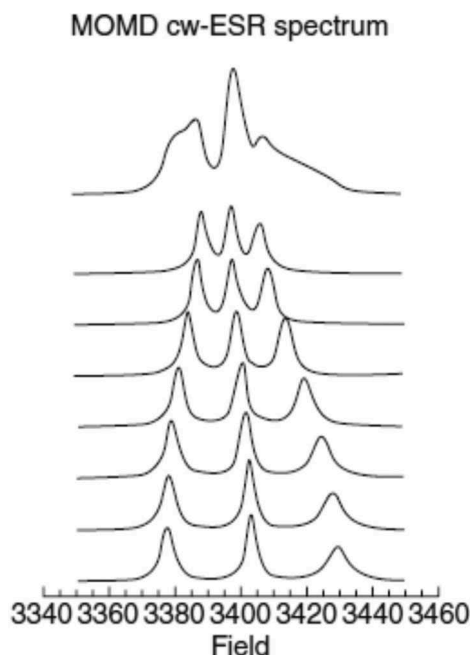


Figure 7. Simulated absorption 9 GHz ESR spectra from a nitroxide dissolved in an anisotropic solvent as a function of the angle, θ , between the director and the external magnetic field. Starting with the second trace, the θ values are 90° , 75° , 60° , 45° , 30° , 15° and 0° . The MOMD spectrum is depicted on the top [59].

(FP) of the virus which inserts into the target membrane [81,82]. One studies the ESR spectrum as a function of fusion peptide concentration using lipids spin-labelled at various positions along the chain, and at the headgroup, of the lipid molecule. By plotting the value of the S_0^2 obtained from the MOMD fit to the ESR spectrum versus FP concentration, an S-shaped curve (cf. Figure 8), representing a sharp increase in S_0^2 at a particular concentration to a new plateau value, is obtained. This is taken as a collective effect by the FP's to increase local ordering in the membrane domains to initiate the fusion process. Modified FP's, which are not fusogenic, do not show this effect. This same phenomenon has now been observed by ESR/MOMD for the FP's of several well-known viruses.

Reference [83] is a particularly revealing illustration of this MOMD/ESR method for solving important issues in biology. The focus of that article is a comparison of the fertility-linked conserved trans-membrane protein HAP2/GCS1 (from the protozoa *T. thermophila*), hypothesised to be an ancient gamete fusogen and the HAP2 dengue virus FP, which adopts a protein fold remarkably similar to HAP2/GCS1. Within the scope of a comprehensive study comprising a number of biophysical methods, MOMD/ESR was utilised to show that the dengue virus FP shows the

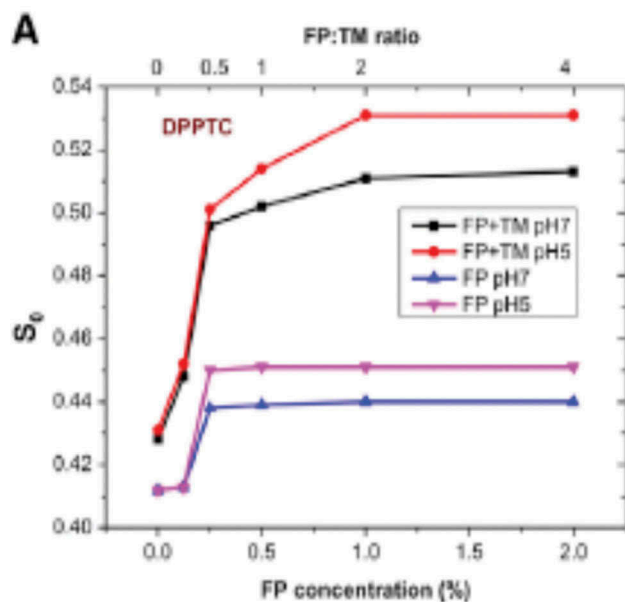


Figure 8. (Colour online) Order parameter, $S_0 = S_0^2$, of dipalmitoylphosphatidyl-tempo-choline versus the influenza haemagglutinin subunit HA2 fusion peptide concentration in 1,2-dimyristoyl-sn-glycerol-3-phosphocholine/1,2-dimyristoyl-sn-glycerol-3-phospho-(1'-rac-glycerol/cholesterol = 40:30:30) multilamellar vesicles with (black, red) or without (blue, pink) 0.5% transmembrane domain (mol:mol) peptide in pH 7 (black, blue) and pH 5 (red, pink) buffer with 150 mM NaCl at 37°C [82].

typical collective increase in the membrane order parameter, S_0^2 . The results support the idea that the *T. thermophila* HAP2 fusion loop participates in membrane fusion during mating. Thus, HAP2 may have arisen from a virus and been key to the origin of eukaryotic sex.

High-frequency ESR

An advance that is important, in general, and very useful for dispersions, in particular, has been the establishment of high-frequency ESR, notably the spectrometer operating at 250 GHz microwave frequency [23,24]. To appreciate the substantial increase in orientational sensitivity at high microwave frequencies, implied by the considerably larger anisotropy of the g-tensor, we show in Figure 9 CSL powder spectra at 9 and 250 GHz [55]; clearly, they differ to a very large extent, with the latter showing the very substantial g-tensor resolution.

Reference [55] illustrates the benefit of using high-frequency ESR to study local ordering in oriented DPPC bilayers and oriented mixed DPPC and dimyristoylphosphatidylserine (DMPS) bilayers. The spin-probe used was CSL, and the sample was oriented

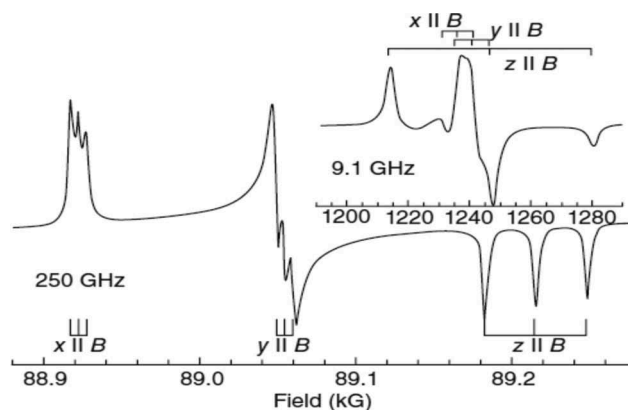


Figure 9. Powder spectra of the CSL probe at 9 and 250 GHz. The short bars denote the field values where absorption occurs when the principal axes (denoted here x , y , z) of the g and A tensors (taken the same) are parallel to the external magnetic field [55].

either parallel or perpendicular to the external magnetic field. Samples in pure DPPC yielded single-component ESR spectra exhibiting axial diffusion (in agreement with the cylindrical shape of CSL) and elaborate local potentials, comprising the terms with $L = 2$, $|K| = 0, 2$ and $L = 4$, $|K| = 0, 2$. To appreciate the extent of the information obtained we show in Figure 10 several un-normalised probability distributions, $\exp(-u(\beta, \gamma))$, where $u(\beta, \gamma)$ are the

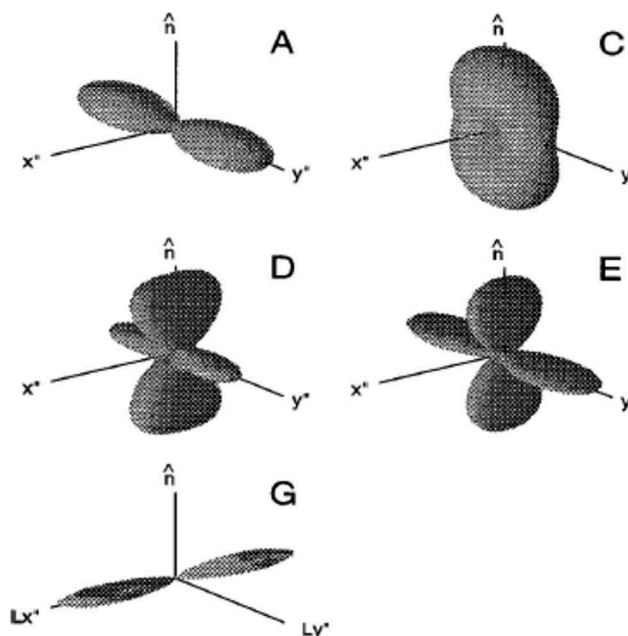


Figure 10. Un-normalised probability distributions, $\exp(-u(\beta, \gamma))$, corresponding to the potentials depicted in columns A, C, D, E and G of Table 2, which are best-fit potentials determined in Reference [55]. \hat{n} is the normal to the bilayer plane [55].

Table 1. Character table of the D_{2h} point-group. [53]

	E	C_2 (z)	C_2 (y)	C_2 (x)	σ i	σ (xy)	σ (xz)	σ (yz)	Linear rotations	quadratic
A_g	1	1	1	1	1	1	1	1		x^2, y^2, z^2
B_{1g}	1	1	-1	-1	1	1	-1	-1	R_z	xy
B_{2g}	1	-1	1	-1	1	-1	1	-1	R_y	xz
B_{3g}	1	-1	-1	1	1	-1	-1	1	R_x	yz
A_u	1	1	1	1	-1	-1	-1	-1		
B_{1u}	1	1	-1	-1	-1	-1	1	1	z	
B_{2u}	1	-1	1	-1	-1	1	-1	1	y	
B_{3u}	1	-1	-1	1	-1	1	1	-1	x	

Table 2. Order parameters from NLLS fits of ESR spectra from oriented DMPC bilayers doped with CSL. The potentials depicted correspond to the un-normalised probability distributions shown in Figure 10 [55].

coefficient of $u(\beta, \gamma)$	A	C	D	E	G
c_0^2	-0.81	1.40	2.00	0.90	-5.16
c_2^2	-1.47	-1.17	-1.50	-0.84	2.13
c_4^0			0.0	0.89	0.0
c_2^4			1.0	1.15	-2.28
c_4^4			0.0	0.0	0.0
dc_{20}					-20.0

best-fit SRLS potentials given in Table 2. Cases A and B (not shown) give the best fit for the gel phase of 80:20 mol% DMPC:DMPS.

A second spectral component appeared upon adding DMPS to DPPC. That component exhibited a new ordering-related feature – strong local biaxiality at the position of the CSL probe, ascribed to inefficient packing between CSL and DMPS. Cases C, D, E, and G of Figure 10 were tried to fit the spectra of this component from 100% DMPS. Only case G, which involves a distribution of local biaxial director axes \hat{n}_L relative to the macroscopic director axis \hat{n} , was found to be successful. The orientation of \hat{n}_L relative to \hat{n} is given by the polar angles (ξ, ζ) . Each orientation is weighted by a probability factor $\exp(-V(\xi, \zeta)) \sin \xi \, d\xi \, d\zeta$. For the present case one may choose $V = -dc_{20} \cos \xi^2$, where dc_{20} is the new parameter in the fit. The ESR spectrum for a given macroscopic orientation is then the sum of the spectra due to all orientations of \hat{n}_L . Such biaxiality was predicted by MD simulations, but previously not observed experimentally. To our knowledge, no other method has provided information on local ordering in phospholipid bilayers at this level of detail.

2D-ELDOR

The other important event, advancing significantly the research of phospholipid dispersions, has been the development of 2D-ELDOR [25–28]. Spectra from this technique are substantially more sensitive to molecular structure and dynamics than CW ESR spectra.

Thermotropic liquid crystals. 2D-ELDOR has been instrumental in showing that SLE-based SRLS [42] rather than the standard liquid crystal SLE theory [16] is the appropriate approach to use even for thermotropic liquid crystals. The upper row of Figure 11 shows experimental 2D-ELDOR magnitude spectra obtained from the rigid CSL probe dissolved in the liquid crystalline phases of 4O,8 [49]. The middle row shows the best-fit spectra calculated with SRLS, and the lower row shows the best-fit spectra calculated with the standard SLC model. The SRLS simulations reproduce the experimental spectra substantially better than those of the SLC. (See also Reference 50, which is the 2D-ELDOR study of the small and weakly aligned probe PDT in 4O,8; it also leads to much better fits with the SRLS model.) While the standard model required an unduly large rotational anisotropy of CSL, this was no longer required by SRLS. Thus, in this case, and undoubtedly in other cases where the dynamic structure of LCs is studied with ESR, internal SRLS ordering has to be accounted for in addition to the external LC ordering. The local structure potential is expressed in terms of the real linear combinations of the Wigner rotation matrix elements for $L = 2, |K| = 0, 2$ with coefficients c_0^2 and c_2^2 . The LC potential is also expressed in terms of these real Wigner rotation matrix elements with coefficients a_0^2 and a_2^2 . The coefficients determined in Reference [49] for the various phases of 4O,8 are given in Table 3(a). The two types of potentials differ in shape, magnitude and temperature-dependence; this is expected in view of their different nature. Table 3(b) shows the coefficients a_0^2 and a_2^2 obtained with the SLC instead of SRLS analysis; they differ substantially from their counterparts in Table 3(a), indicating that in this case, the SLC analysis is oversimplified. Clearly, the local ordering is well determined in this case.

Note that this was a temperature-dependent study (ca. 25–100 °C) that covered many liquid crystalline phases: Isotropic (I), Nematic (N), Smectic A (S_A), Smectic B (S_B), and crystal (C). One sees from Table 3(a) that the cage potential varies from ca. 1 kT in the isotropic phase to greater than 2 kT in the N and S_A phases, with an abrupt drop to about 0.2 kT in the S_B and C phases. Concomitant with this drop at the S_A - S_B transition is an almost comparable increase in the orienting potential associated with the macroscopic alignment. This is consistent with a freezing-in of the smectic structure at this transition. The cage relaxation rate given by R^c in Table 4 is of $10^7 \, s^{-1}$ in the I and N phases. It drops somewhat in the S_A phase, but there is a greater than an order of magnitude drop in R^c for the S_B and C phases to about $10^5 \, s^{-1}$, consistent with a freezing-in of the smectic structure. The overall CSL

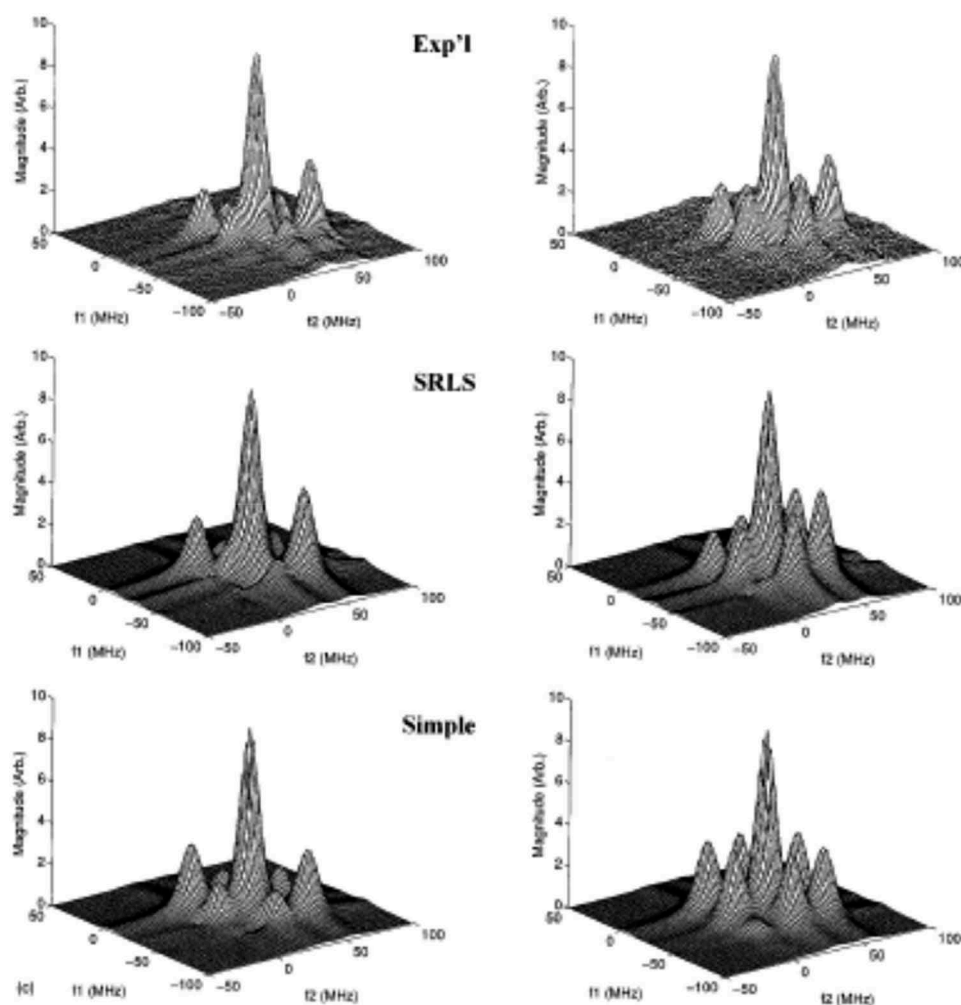


Figure 11. Experimental and simulated 2D-ELDOR spectra of CSL in the smectic A phase of 40,8 at 59°C. Left (right) column is for a mixing time of 200 (300) ns. Top spectra are experimental, middle spectra are SRLS simulations, and bottom spectra are standard model simulations [49].

Table 3a. Best-fit LC potentials (coefficients a_0^2 and a_2^2) and cage potentials (coefficients c_0^2 and c_2^2) obtained with NLLS SRLS data-fitting of 2D ELDOR spectra from 40,8 doped with CSL at the temperatures specified [49].

Phase	T(°C)	a_0^2	a_2^2	c_0^2	c_2^2
<i>I</i>	96.2	1.10	0.96
<i>I</i>	91.0	1.04	0.95
<i>I</i>	86.1	0.73	0.96
<i>I</i>	80.2	0.73	0.96
<i>N</i>	73.1	1.93	1.46	1.85	0.62
<i>N</i>	70.2	2.15	0.86	2.00	0.62
<i>N</i>	67.5	2.50	1.12	1.84	0.81
<i>N</i>	65.0	2.74	1.27	1.72	0.62
<i>S_A</i>	59.1	3.57	0.84	2.26	0.82
<i>S_A</i>	56.4	3.79	1.16	2.23	0.78
<i>S_A</i>	53.6	4.15	1.44	2.25	0.79
<i>S_A</i>	50.8	4.68	1.17	1.62	0.74
<i>S_B</i>	44.4	7.49	-0.62	0.215	-0.029
<i>S_B</i>	40.7	7.78	-0.50	0.191	-0.003
<i>S_B</i>	38.1	7.55	-0.58	0.246	-0.010
<i>S_B</i>	35.2	7.62	-0.88	0.451	-0.027
<i>C</i>	29.1	7.61	-0.86	0.200	-0.004
<i>C</i>	24.6	7.96	-1.40	0.075	-0.002

Table 3b. Best-fit LC potentials (a_0^2 and a_2^2) obtained with NLLS standard LC model fitting of the 2D ELDOR spectra obtained in Reference [49] at 59°C, 65°C and 91°C [49].

T(°C)	a_0^2	a_2^2
91
65	2.67	-0.99
59	3.68	1.81

motion is considerably slower than the local-structure dynamics (ca. $10^8 - 10^9 \text{ s}^{-1}$), consistent with the application of the SRLS model.

These results show the great insights obtainable from 2D-ELDOR studies on ordered fluids.

Lytropic liquid crystals

2D-ELDOR spectra for vesicles of pure DPPC and GA-containing DPPC bilayers, using 16-PC as probe are shown in Figure 12A [31]. It can be seen that the

Table 4. Best-fit global motions rates, R^c , and local motional rates, R_{\parallel}^0 and R_{\perp}^0 , which correspond to the data shown in Table 3a [49].

Phase	T(°C)	$R_{\parallel}^0 \times 10^{-9}(s^{-1})$	$R_{\perp}^0 \times 10^{-9}(s^{-1})$	$R^c \times 10^{-7}(s^{-1})$
<i>l</i>	96.2	0.62	0.119	2.03
<i>l</i>	91.0	0.57	0.094	0.90
<i>l</i>	86.1	0.53	0.088	0.43
<i>l</i>	80.2	0.49	0.080	0.48
<i>N</i>	73.1	0.77	0.138	1.08
<i>N</i>	70.2	0.68	0.131	1.40
<i>N</i>	67.5	0.65	0.121	1.01
<i>N</i>	65.0	0.54	0.101	0.84
<i>S_A</i>	59.1	2.37	0.081	0.33
<i>S_A</i>	56.4	2.36	0.086	0.32
<i>S_A</i>	53.6	2.48	0.077	0.33
<i>S_A</i>	50.8	2.33	0.083	0.28
<i>S_B</i>	44.4	3.23	0.150	0.022
<i>S_B</i>	40.7	2.86	0.115	0.021
<i>S_B</i>	38.1	2.77	0.150	0.022
<i>S_B</i>	35.2	2.09	0.141	0.015
<i>C</i>	29.1	2.00	0.124	0.010
<i>C</i>	24.6	1.98	0.137	0.000

spectra shown in part A (2D-ELDOR) are substantially more sensitive to the addition of GA than the spectra shown in part B (CW ESR). The system consisting of DPPC and DPPC-GA vesicles was studied quantitatively with both CW ESR [66,70] and 2D-ELDOR [32]. While CW ESR provided useful information associated with lipid-peptide interactions, detailed information could only be obtained using 2D ELDOR [32].

Pure DPPC was found in Reference [32] to exhibit fast motion and weak ordering, as expected for bulk lipid. When GA was added an additional component, exhibiting much stronger ordering and slower local motion, appeared. It was interpreted as ‘boundary lipid’, in agreement with References 66 and 70.

It was found in Reference [32] that ‘ γ -ordering’ (meaning that the largest Saupe order parameter in absolute magnitude is $S_{\gamma\gamma}$) and slow local motion characterise the ‘boundary lipid’. This points to a dynamic bending at the end of the acyl chains, as they coat the GA molecule. Thus, new ordering-related insight into the effect of GA insertion in membranes was obtained with 2D-ELDOR studies on vesicle dispersions.

Another example where 2D-ELDOR provided important information that could not be obtained with CW ESR is the study described in Reference [84]. The ‘full Sc-’ method (detailed description appears in Reference [85]) was used to elucidate structural changes in plasma membrane vesicles isolated from RBL-2H3 mast cells upon antigen cross-linking of IgE receptors (IgE-Fc ϵ RI). The results demonstrate the coexistence of liquid-ordered (L_o) and liquid-disordered (L_d) components. It was found that upon cross-linking the membrane becomes more disordered; this feature is important from a biological point of view. The changes revealed are small, showing that

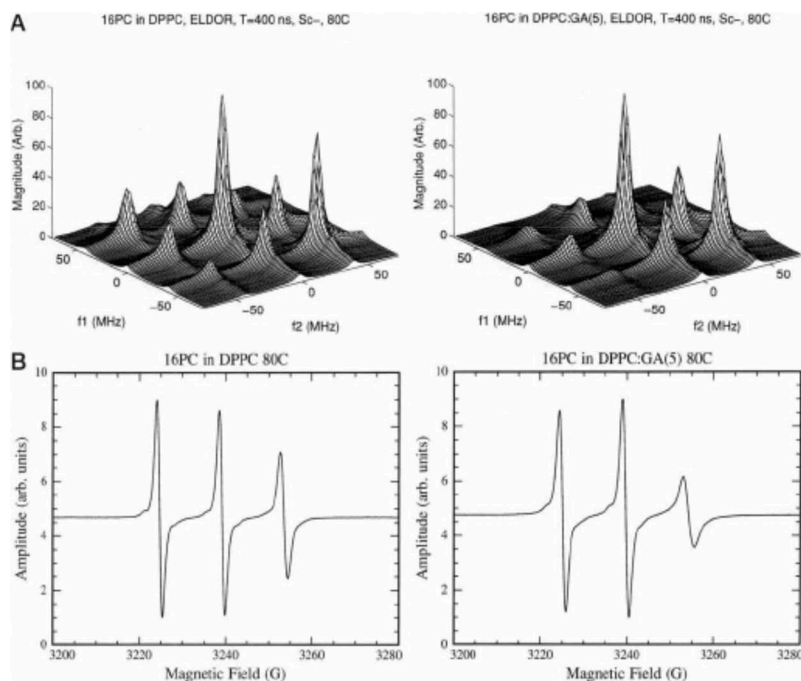


Figure 12. 2D-ELDOR S_c - spectra obtained for DPPC bilayers (right) and DPPC bilayers containing GA (left) at 80°C for a mixing time of 400 ns (part A); corresponding CW ESR spectra (part B) [31].

2D ELDOR analysed with the ‘full Sc-’ method can be applied to study complex systems where physical processes bring about subtle changes.

Multifrequency ESR

Our last example relates to multifrequency ESR, which is particularly useful when the system studied exhibits complex motions that are timescale-separated. Reference [35] provides a typical example. CW ESR spectra from dispersions of pure DPPC, and DPPC:cholesterol in a 1:1 molar ratio, were acquired at 9 and 250 GHz microwave frequency. The probe used was 16-PC. Figures 13A and 13C (13B and 13D) show the temperature-profiles of the diffusion rate constant, R_{\perp} , and the order parameter, $S_0 \equiv S_0^2$, obtained at 250 (9) GHz using MOMD. The results obtained at the two spectrometer frequencies differ substantially. Consistent results were obtained by analysing the 9 GHz spectra with SRLS (not shown). The discrepancy illustrated in Figure 13 is ascribed to the fact that at 250 GHz only the fast reorientation of the probe affects the analysis as the overall motion is too slow to affect the spectrum, hence MOMD suffices, whereas at 9 GHz the slow reorientation of the lipid in the membrane also affects the spectrum, hence SRLS is required. Thus,

Figures 13A and 13C directly reflect the faster probe motion, whereas Figures 13B and 13D reflect the composite motion of the fast and slow modes that require an SRLS analysis to separate them (note that foreknowledge of the 250 GHz MOMD fit to the faster local motion [35] is required). This is an example of the need for a multifrequency CW study to elicit the details of a complete SRLS analysis. Figure 13C shows a phase transition between 40°C and 41°C for pure DPPC; no phase transition is observed for the DPPC/cholesterol mixture. This is consistent with DPPC exhibiting a gel phase below 40°C and an LC phase above 41°C, whereas the DPPC-cholesterol mixture exhibits an ordered-LC phase [75] throughout the temperature range studied. Note that just the order parameter picked up the phase transition occurring in pure DPPC.

Local ordering in biological macromolecules from SRLS/ESR analysis

Reference [7] examines the sensitivity of the SRLS analysis to the physical parameters entering this model. Simple limits of SRLS are discussed. In the Fast Internal Motion (FIM) model the local motion is in the extreme motional narrowing limit. Partially

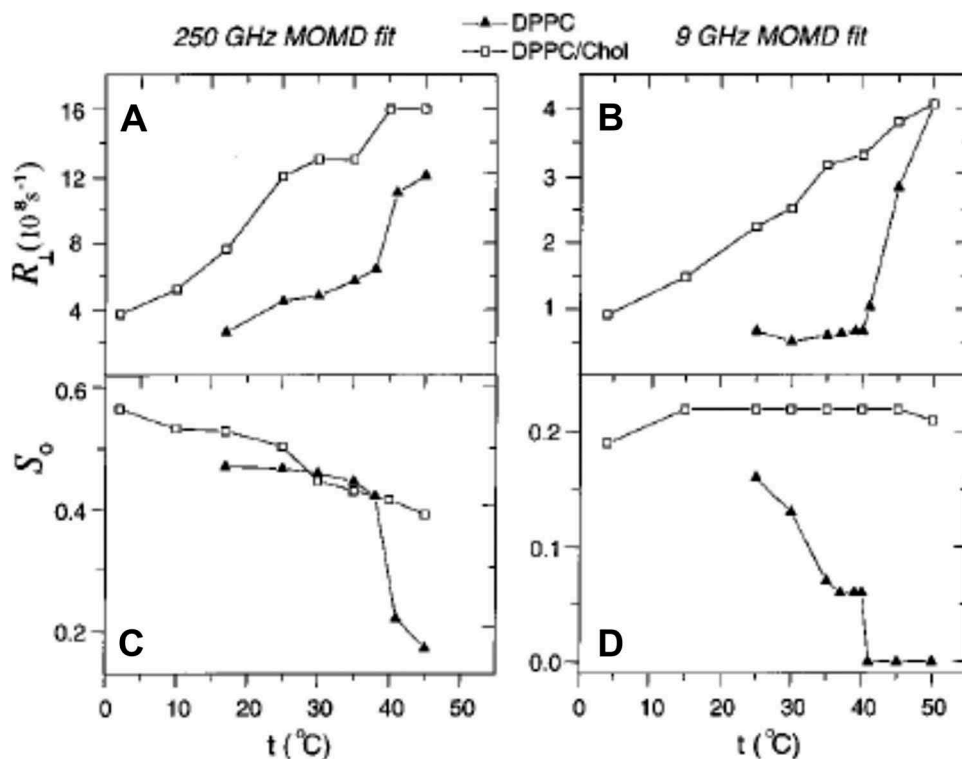


Figure 13. Diffusion rate constant, R_{\perp} , and order parameter, S_0^2 , from 16-PC in DPPC vesicles as a function of temperature at 250 GHz microwave frequency (parts A and C) and as 9 GHz microwave frequency (parts B and D). The experimental ESR spectra [35] were analysed with MOMD [30]. The filled triangles correspond to pure DPPC and the open circles correspond to the DPPC/cholesterol mixture.

averaged magnetic tensors are characterised by an ‘effective’ order parameter, and the slower global motion is described in terms of diffusion constant(s). The Very Anisotropic Rotation (VAR) model just has a fast R_{\parallel}^o motion and slow R_{\perp}^c motion but no local ordering. The Averaged Hamiltonian model is the simple limit where both FIM and MOMD models apply. These simplified models typically yield inaccurate parameters as illustrated in Table 5 from Reference [7], as well as Figure 13. The row designated ‘SRLS’ comprises the parameters used to generate a 9 GHz reference spectrum. The rows designated ‘MOMD’ and ‘FIM’ comprise the best-fit parameters obtained with MOMD and FIM fitting, respectively, of the reference spectrum. It can be seen that MOMD provides the composite of both motions, whereas FIM is inapplicable.

SRLS applied to DNA oligomers. The SRLS schematic in Figure 14 depicts a DNA fragment labelled with a nitroxide [44]. The DNA molecule executes overall diffusion with rate constants R_{\parallel}^c and R_{\perp}^c ; the nitroxide executes restricted internal diffusion with rate constants R_{\parallel}^o and R_{\perp}^o . The local director, C' , given by the average orientation of the spin-labelled side-chain, is represented by the symmetry-axis of the cone; $\beta_{cc'}$ is the tilt angle between the director frame, C' , and the global diffusion frame, C .

Different nitroxide labels featuring different-length tethers attached to DNA oligomers of several lengths were used and analysed with SRLS. The correlation times for the global tumbling were obtained from hydrodynamic theory, enabling the determination of the local motional ordering and dynamics by fits to the ESR spectra. Two types of spectra were found. In one type the spin labels are trapped in a highly restricted/slow motional site and have a stronger interaction with the base than those in the other site. In general, R_{\perp}^o becomes slower as the size of the oligomer increases, which may be a manifestation of collective modes of motion of the DNA.

Table 5. Upper row: reference SRLS spectrum defined by $R_{\parallel}^c = R_{\perp}^c = 10^7 \text{ s}^{-1}$, $R_{\parallel}^o = R_{\perp}^o = 10^8 \text{ s}^{-1}$, $c_0^2 = 3.00$ ($S_0^2 = 0.61$) and intrinsic linewidth $W_1 \equiv (T_2^*)^{-1} = 2 \text{ G}$. **Middle row:** best-fit spectrum obtained with MOMD-fitting of the target spectrum. **Lower row:** best-fit spectrum obtained with FIM-fitting of the target spectrum. The microwave frequency was 250 GHz in these calculations [7].

Model	$R_{\perp}^c = R_{\parallel}^c \times 10^{-7} (\text{s}^{-1})$	$R_{\perp}^o = R_{\parallel}^o \times 10^{-8} (\text{s}^{-1})$	c_0^2	S_0^2	W_1 (G)
SRLS	1	1	3	(0.61)	2
MOMD		0.53	1.6	(0.36)	1.4
FIM	2.6			0.86	1.1

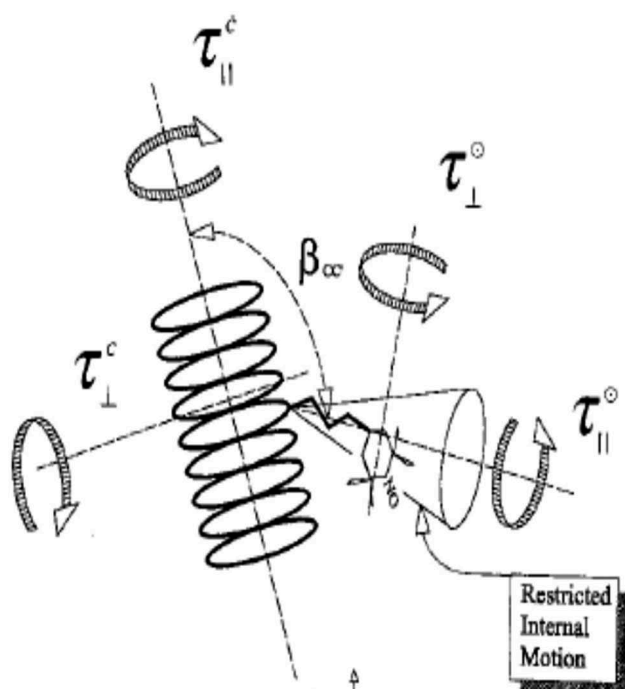


Figure 14. Schematic of a nitroxide-labelled DNA oligomer for the SRLS model. The various parameters are specified in the text [44].

SRLS applied to T4 lysozyme. Several ESR studies of nitroxide-labelled T4L have been performed in the 1996–2010 time-frame [36,43,86,87]. The experiments became more extensive and the analysis more detailed with time. We will discuss in some detail the last study [43], following a brief summary of the earlier work.

Thirty single cysteine substitution mutants of T4L were prepared in Reference [86] (year 1996) to systematically investigate the relationship between nitroxide side-chain mobility and protein structure. ESR spectra were acquired at 9 GHz microwave frequency. The structural perturbations were shown to be small at solvent-exposed sites. The primary determinants of nitroxide side-chain mobility were found to be tertiary-structure-associated interactions which exert local restrictions, and backbone dynamics. In Reference [87] (year 1999) ESR spectra from T4L lysozyme labelled with nitroxide at positions 44 and 69 were acquired in the 10–35°C temperature range, and at 9 and 250 GHz microwave frequency. The 250 GHz spectra were analysed with MOMD to obtain the internal dynamic and structural parameters. The results obtained were used as fixed input to the SRLS analysis of the 9 GHz spectra, where only the global motional rate, R^c , was allowed to vary. For both sites, a single component was detected at higher temperatures and two components were detected at lower temperatures.

In aqueous solution, three components were found for R1 and two for R2. One component exhibited slower local motion and strong local ordering. Its population decreased with increasing temperature. This component was found to be more populated in the R2 spectra. The local ordering was associated with spatial restrictions exerted by the protein surface. The other two sites exhibited faster local motion and weaker local ordering; they correspond to conformers having less or no interaction with nearby residues.

Extensive information on local potentials and associated order parameters was obtained. To appreciate the insights gained one should examine collectively the parameters associated with ordering, motion and site-occupancy. Figure 18 provides such a view for the aqueous solutions.

Table 6 shows as an example the potential coefficients, c_0^2 and c_2^2 , and the order parameters, S_0^2 and S_2^2 , defined in terms of these coefficients for the local motion of the R1 side chain of residue 72. In agreement with Figure 18, the strength of the potential (c_0^2 and S_0^2) varies little. However, the rhombicity of the potential (c_2^2 and S_2^2) changes substantially with temperature, in evidence of considerable temperature-induced variations in the shape of the potential. The results obtained

for R1 at site 131, and R2 at both sites, in the Ficoll-containing solutions are described in Reference [43].

Reference [43] describes the most extensive investigation of the dynamic structure of a protein as elucidated with ESR lineshape analysis reported so far. It may be considered as a paradigm of what can be learned about internal protein mobility, in general, and local ordering at mobile sites in proteins, in particular, using the SRLS analysis of multifrequency ESR.

Local ordering in proteins dissolved in aqueous solution from SRLS/NMR relaxation analysis

The magnetic interactions associated with the ^{15}N , ^{13}C and ^2H nuclei, typically used as probes, are on the order of $5 \times 10^5 \text{ s}^{-1}$. The tumbling rate of a small globular protein is approximately $5 \times 10^7 \text{ s}^{-1}$ in aqueous solution. Thus, NMR relaxation for globular proteins is necessarily in the motional narrowing regime. One may solve the appropriate Smoluchowski equation (which is an easier task than solving the full SLE) to obtain time-correlation functions which are Fourier-transformed into spectral densities and then used in standard motionally narrowed relaxation theory. The consensus in the field is that one may take the magnetic

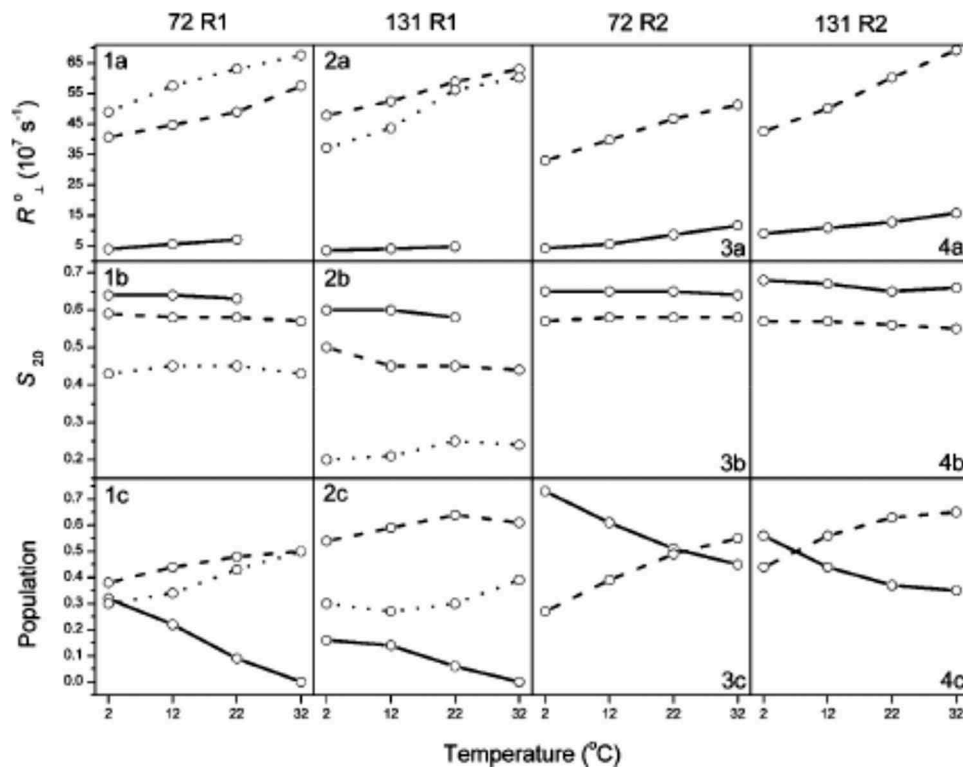


Figure 18. Best-fit local motional rate constant, R_{\perp}^0 , axial order parameter, S_0^2 , and population of the 'immobile' component (solid line), of the 'intermediate' component (dashed line), and the 'mobile' component (dotted line). The best-fit tilt angles between the local diffusion/local ordering frame and the magnetic-tensor frame were determined to be 21° , 20° , 30° and 35° for 72R1, 131R1, 72R2 and 131R2 [43].

Table 6. Best-fit potential coefficients, c_0^2 and c_2^2 , and order parameters, S_0^2 and S_2^2 , for local motion in 72R1 [43].

comp.	T, °C	c_0^2	c_2^2	S_0^2	S_2^2	population
1	2	3.20	0.05	0.64	0.00	0.32
2		3.49	-1.86	0.59	-0.16	0.38
3		3.21	-2.73	0.43	-0.31	0.30
1	12	3.30	0.18	0.64	0.01	0.22
2		3.37	-1.75	0.58	-0.15	0.44
3		2.79	-1.98	0.45	-0.25	0.34
1	22	3.22	0.25	0.63	0.02	0.09
2		3.31	-1.67	0.58	-0.15	0.48
3		2.62	-1.66	0.45	-0.22	0.43
2	32	3.24	-1.66	0.57	-0.16	0.50
3		2.30	-1.30	0.43	-0.20	0.50

anisotropies that enter the theory as uniform and fixed [88].

We have developed the SMLS analysis for NMR relaxation in proteins, in particular for ^{15}N -labelled proteins at the backbone amide position, and deuterium-labelled proteins at the side-chain methyl-moiety position [45–48]. Typical experimental data include ^{15}N T_1 , T_2 and ^{15}N - $\{^1\text{H}\}$ NOE for the ^{15}N - ^1H probe, and ^2H T_1 and T_2 for the C- CD_3 probe [88]. Methods for acquiring spectra which feature all of the N- ^1H bonds or C- CD_3 moieties of a given protein exist [89,90]. Thus, the dynamic structure of the protein may be mapped out at the residue or methyl-moiety level. One obtains from SMLS the relevant relaxation parameters on the basis of the theory given in the Theoretical Summary section. In any given analysis the best-fit SMLS parameter combination is determined by data-fitting. We show below examples of SMLS analyses of ^{15}N -H and C- CD_3 relaxation in proteins which yielded new insights into the local ordering at the sites of these probes.

SMLS applied to ^{15}N relaxation from the third immunoglobulin domain of streptococcal protein G (GB3). Experimental ^{15}N T_1 , T_2 and ^{15}N - $\{^1\text{H}\}$ NOE relaxation parameters of GB3 were acquired in Reference [91] at magnetic fields of 11.7, 14.1, 16.4 and 18.8 T, in the 278–323 K temperature range. These data had been analysed with the MF method where the global motion of the protein is taken as isotropic, and the local ordering at the site of the probe is taken as axially symmetric. Unsatisfactory statistics were obtained in fitting the experimental data; only by forcing axial global diffusion on the analysis, and allowing the ^{15}N chemical shift anisotropy (CSA) to vary, were adequate statistics obtained [92].

We analysed the same data with SMLS in terms of isotropic global motion and rhombic local ordering potential, $u = -c_0^2 D_{00}^2 - c_2^2 (D_{02}^2 + D_{0-2}^2)$ [92]. Rhombic ordering is considerably more important than relatively small deviations from isotropic global motion in affecting the

results, as demonstrated previously [93]. Good statistics were obtained using a constant ^{15}N CSA.

The GB3 potential, u , is a function of the Euler angles Ω_{CM} (Figure 3, with $C' = C$), which represent the transformation from the local director frame, C, to the local ordering frame, M. One has $Z_{\text{C}} \equiv (\text{NH})_{\text{average}}$, $Z_{\text{M}} \equiv C^\alpha - C^\alpha$, $Y_{\text{M}} \equiv \text{NH}$, and X_{M} oriented at 90° to the peptide-bond plane [45–48]. To render this ordering more intuitive we permuted the axes of the M frame so that $Y_{\text{M}} = \text{NH}$ orients preferentially along $Z_{\text{C}} \equiv (\text{NH})_{\text{average}}$; this required transforming c_0^2 and c_2^2 into \hat{c}_0^2 and \hat{c}_2^2 , as delineated in the Appendix of Reference [55].

Figure 19 shows the permuted coefficients as a function of residue number, with the secondary structure of GB3 depicted on the top. As expected, \hat{c}_0^2 is large and positive throughout the polypeptide chain, indicating strong local ordering centred at the average N-H orientation. The coefficient \hat{c}_2^2 is large and negative for the long α -helix of GB3, indicating that the $C^\alpha - C^\alpha$ axis orients perpendicular to $(\text{NH})_{\text{average}}$ to a larger extent than the orientation at 90° to the peptide-bond plane. On the other hand, \hat{c}_2^2 is large and positive for the rest of the polypeptide chain, indicating that the orientation at 90° to the peptide-bond plane orients perpendicular to $(\text{NH})_{\text{average}}$ to a larger extent than the $C^\alpha - C^\alpha$ axis.

The form/symmetry of local potential/local ordering at the site of the probe is determined by the immediate internal protein surroundings. Our results show that the long α -helix imposes on the relevant N-H bonds

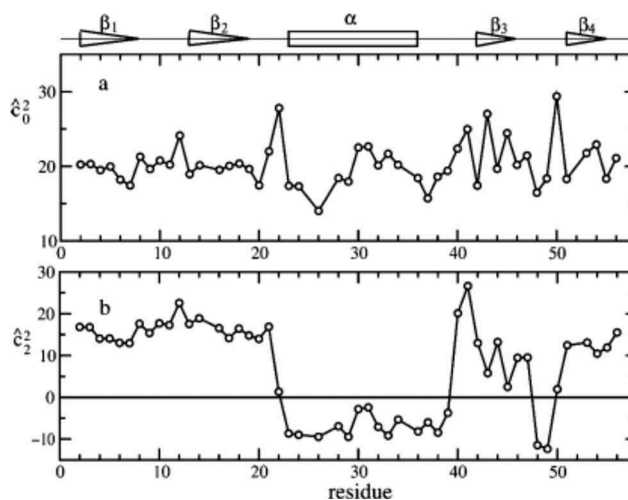


Figure 19. Best-fit axial, \hat{c}_0^2 (a), and rhombic, \hat{c}_2^2 (b), coefficients of the potential given by $u = -\hat{c}_0^2 D_{00}^2 - \hat{c}_2^2 (D_{02}^2 + D_{0-2}^2)$ [92]. Experimental ^{15}N relaxation parameters of GB3 from Reference [91].

a rhombicity consistently different from that experienced by all of the other N–H bonds of GB3. This indicates that while generally the form/symmetry of the local potential is largely determined by residue-specific factors, in some cases the secondary structure context dominates.

SRLS applied to ^2H relaxation from the complex of Ca^{+2} -calmodulin with the peptide smMLCKp (CaM). Experimental ^2H T_1 and T_2 data from the C–CD $_3$ groups of CaM acquired at 14.1 and 17.6 T and 288–320 K in Reference [94] were subjected to SRLS analysis [95]. Rhombic local potentials with $L = 2$, i.e. coefficients c_0^2 and c_2^2 , were determined. The analysis described in Reference [95] identified features specific to given methyl groups and methyl sites. The following observation is of particular interest. By plotting the parameter $|c_0^2|$ as a function of methyl type – black circles in Figure 20 – we found that the average value of $|c_0^2|$ is 1.0 for alanine, 0.5 for methionine, and 0.76 for all of the other methyl types (black-dashed lines in Figure 20). Additional proteins yielded similar results (unpublished results).

The MF analysis of the same data was based on S^2 given by Equation (25) to be the product of the effects of two types of motions: very rapid methyl group spinning (or S_M^2), and slower C–CD $_3$ motion (or S_{axis}^2) [94]. S_M^2 was set equal to $[1.5 \cos(109^\circ)^2 - 0.5]^2 = 1/9$, where 109.5° is the tetrahedral angle; S^2 was thus given by the expression $S_{axis}^2 \times (\frac{1}{9})$. The S_{axis}^2 of CaM, taken from

Reference [94], is depicted in Figure 20 by the red circles. It was found to cluster into three groups centred at approximately 0.78, 0.35 and 0.58 [96]. Other proteins yielded similar S_{axis}^2 clustering [97]. The S_{axis}^2 is conceived as an ‘amplitude of motion’; as such it is considered suitable for calculating ‘residual conformational entropy’ [58]. The three classes of S_{axis}^2 values are taken to imply three classes of conformational entropy in proteins [97], reflecting on the microscopic nature of heat capacity in proteins, and pointing to an unexpected explanation of the low-temperature glass-transition of proteins [96].

The MF method [56] is a simple one [46–48]. Its main parameter, S^2 , clearly must be regarded as an imprecisely defined composite; deriving conformational entropy from it is perhaps appropriate in the limit where $S^2 \cong (S_0^2)^2 \rightarrow 1$ and the local motion is very fast (see discussion after Equation (26), and Reference [7]). The $S_{axis}^2 = 9 \times S^2$ with average values in the range of 0.58–0.78, is far outside this limit. Hence, ‘entropy’ derived from S_{axis}^2 is a vague quantity, certainly not suitable as a basis for such far-reaching conclusions.

The 1.0, 0.5 and 0.76 trend in the SRLS parameter $|c_0^2|$ (Figure 20) is empirical in nature. Nevertheless, it is consistent with the alanine methyl groups, located in proximity to the rigid protein backbone, exhibiting substantially rhombic ordering (relatively large $|c_2^2|$). The methionine methyl groups exhibit nearly axial

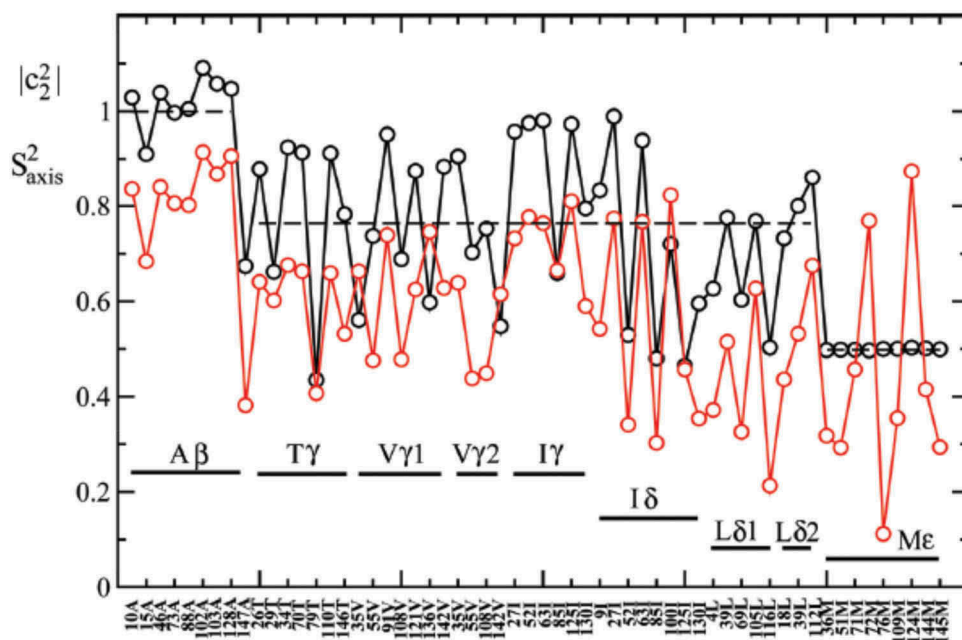


Figure 20. (Colour online) Best-fit values of $|c_2^2|$ (black circles) and average values of $|c_2^2|$ for alanine, methionine and the other methyl-groups of CaM (black-dashed lines) [95], and S_{axis}^2 (red circles) [94], as a function of methyl type, at 295 K.

ordering (small $|c_2^2|$), as they are located at a considerable distance from the backbone in a less spatially restricting, on average nearly axially symmetric, environment. All of the other methyl groups are in-between these limiting cases. This interpretation of the empirical trend illustrated in Figure 20 is clearly more plausible than the MF interpretation of having discovered three classes of entropy in proteins [97]. Conformational entropy that is physically meaningful is derived in SRLS from the probability distribution $P_{eq} \propto \exp(-u)$, where u is the SRLS potential. An example associated with methyl-group dynamics in the context of ligand-binding) appears in Reference [98]; as expected, the SRLS-derived changes in conformational entropy upon ligand-binding differ qualitatively from their S_{axis}^2 -derived counterparts.

Local ordering in polycrystalline samples from MOMD/NMR analysis

The analysis of deuterium lineshapes from polycrystalline samples emerged as a particularly useful tool for studying microsecond-millisecond motions in the solid-state [99,100], which are often relevant from a biological point of view. Various dynamic models have been developed in the course of the years. Many are of the MSM type, comprising simple jump-type modes as constituents – cf. Reference [8]. In some

cases, relatively simple Smoluchowski models have been developed [9,10].

We developed MOMD for ^2H NMR lineshape analysis of spectra from polycrystalline proteins [8,37–40]. The power of this approach, in particular in the context of the local ordering, is illustrated below.

MOMD applied to the chicken villin headpiece sub-domain (HP36). This protein was studied previously in Reference [101]. The methyl groups of residues L75, L61, L69 and V50 were selectively deuterated, and quadrupole echo ^2H spectra were acquired in the temperature range of 250–298 K. Figure 21 shows the experimental spectra (red) and their calculated counterparts (blue) obtained using an MSM model. The latter features very fast 3-site hops around $C_\gamma-C_\delta$, jumps of $C_\beta-C_\gamma$ with rate k_{arc} along an arc of length l , and rotamer exchange modelled as $C_\beta-C_\gamma$ jumps with rate k among the corners of a tetrahedron (equilateral triangle) with populations $w:1:1:1$ ($w:1:1$) for leucine (valine). The length of the arc l , together with the population w , in different contexts for leucine and valine, might in some indirect way represent local ordering. Comparing valine and leucine is difficult. Thus, although the fit between calculated and experimental spectra in Figure 21 is good, important aspects of the interpretation, particularly with respect to the local ordering, are problematic.

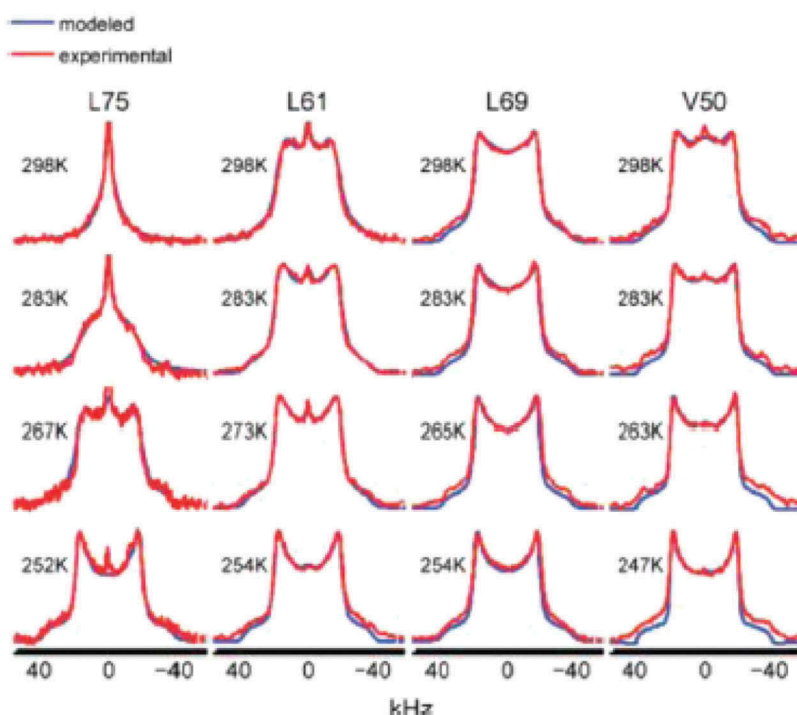


Figure 21. (Colour online) Experimental (red) and calculated (blue) ^2H lineshapes obtained from the selectively deuterated methyl groups L75, L61, L68 and V50 of HP36, using the MSM model discussed in the text [101].

Figure 22 shows the best-fit MOMD ^2H lineshapes [8]; the agreement with the experimental spectra (red traces in Figure 21) is good. The local ordering is given by a rhombic $L = 2$, $|K| = 0, 2$ potential with coefficients c_0^2 and c_2^2 , and the local motion by an axial diffusion tensor with rate constants $R_{\perp} = 1/(6\tau_{\perp})$ and $R_{\parallel} = 1/(6\tau_{\parallel})$. As expected, c_0^2 decreases with increasing temperature. We found that c_2^2 increases with increasing temperature [8]. This is interpreted in terms of degrees of freedom that contribute to the rhombicity of the potential being ‘frozen’ at the lower temperatures. We consider the MOMD-based interpretation, in particular as it refers to the local ordering, insightful.

MOMD applied to medium-size molecules. Reference [37] describes the application of MOMD to C-CD₃ dynamics in the polystyrene-adsorbed Ac-LKKLLKLLKLLKL-OH peptide, and N-CD₃ dynamics in polycrystalline dimethylammonium tetraphenylborate. C-D dynamics in the Hhal methyl-transferase target DNA, and in phase III of benzene-6-hexanoate, were also studied. In all of the cases rhombic $L = 2$, $|K| = 0, 2$ ordering potentials with coefficients c_0^2 and c_2^2 were determined. The ordering in the different systems studied, including HP36, was

compared on the basis of c_0^2 and c_2^2 values and their temperature-dependence; differences in local potential strength and symmetry were revealed.

MOMD applied to deuterated methyl-moiety dynamics in amyloid-A β_{40} fibrils. In Reference [39] MOMD was applied to C-CD₃ moieties in dry and hydrated 3-fold-symmetric and 2-fold-symmetric amyloid-A β_{40} fibrils, and protofibrils of the D23N mutant, using experimental data from Reference [102]. The methyl moieties of L17, L34, V36 (C-CD₃) and M35 (S-CD₃) served as probes. Experimental quadrupole echo ^2H NMR spectra were acquired in the 147–310 K temperature range (blue traces in Figure 23). Using the MSM model employed for HP36, and in addition imposing linearity on the temperature dependence of the major parameters, the calculated spectra coloured in red were obtained. The agreement between the calculated and experimental spectra is very good.

For M35 in the hydrated fibrils of both amyloid-A β_{40} polymorphs, an abrupt spectral change occurs between 258 and 274 K [102]. This was interpreted in terms of the methyl moiety of methionine 35 exhibiting leucine-type rotamer-exchange below 258 K and valine-type rotamer-exchange above 274 K.

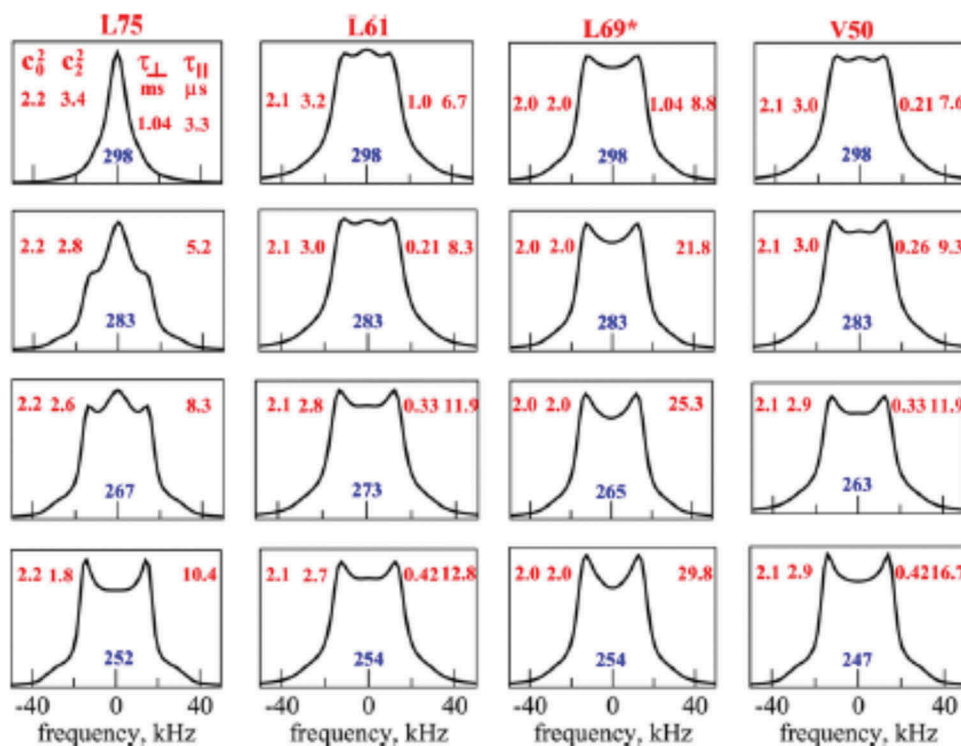


Figure 22. (Colour online) ^2H MOMD lineshapes calculated with the best-fit potential coefficients, c_0^2 and c_2^2 , and correlation times for local motion, τ_{\perp} and τ_{\parallel} , depicted in the figure. The tilt angle, β_{MQ} , between the principal axes of the local ordering/local diffusion and quadrupolar tensors is 110.4° or 69.6° , except for L69 where it is 120° . Both angles are standard stereo-chemical features [8]. These spectra are best-fits to the experimental spectra (red traces) of Figure 21.

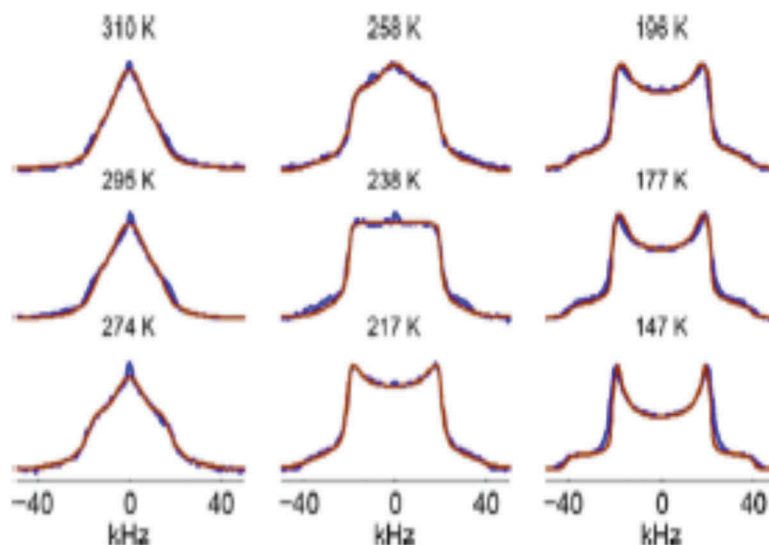


Figure 23. (Colour online) Experimental ^2H lineshapes from the methyl group of M35 in the hydrated threefold-symmetric $\text{A}\beta_{40}$ fibrils at the temperatures depicted in the figures (blue), and best-fit calculated lineshapes (red), from Reference [102].

We analysed the same experimental spectra with MOMD [39]. As for HP36, we allowed for rhombic $L = 2$ ordering potential with coefficients c_0^2 and c_2^2 , axial local diffusion with rate constants R_{\parallel} and R_{\perp} , and ordering tensor tilt given by β_{MQ} . The best-fit MOMD lineshapes are shown in Figure 24; the best-fit parameters appear in Reference [39]. The agreement between calculated and experimental lineshapes is good. All of the best-fit parameters have physically

reasonable values (the deviation of β_{MQ} from standard stereo-chemistry is associated with the simplicity of the local potential). The diffusion rate constant, R_{\parallel} , exhibits Arrhenius-type temperature-dependence and yields a reasonable activation energy of 5.9 kJ/mol; R_{\perp} exhibits limited temperature-dependence.

The abrupt change in the experimental lineshape between 258 and 274 K manifests itself as an abrupt change in the form of the local potential and in β_{MQ} ;

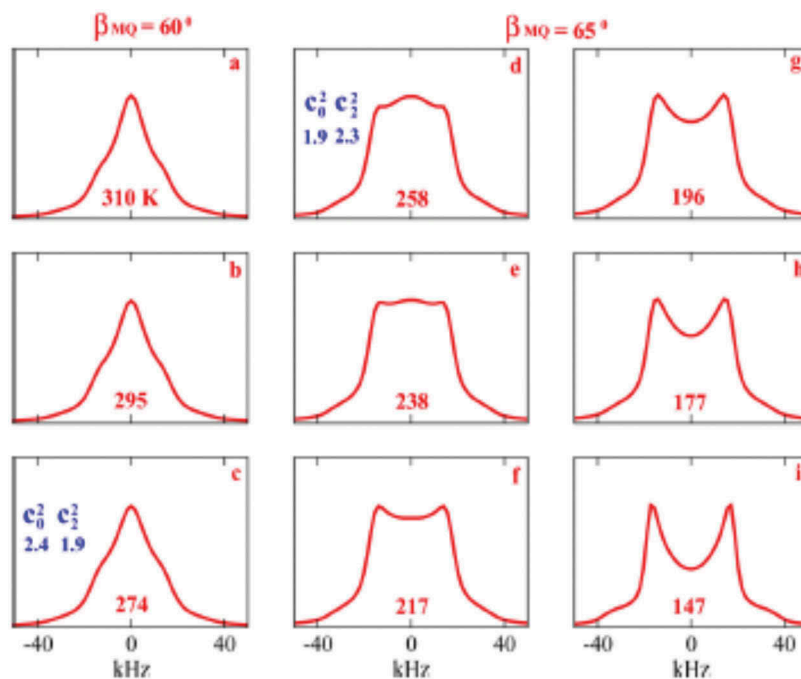


Figure 24. (Colour online) Best-fit MOMD spectra reproducing the experimental ^2H lineshapes from the methyl group of M35 in the hydrated threefold-symmetric $\text{A}\beta_{40}$ fibrils (blue traces in Figure 23). The results obtained at 258 and 274 K, between which the abrupt spectral change occurs, are depicted. $\log R_{\perp}$ is 2.2 throughout, and the effective quadrupole constant is 58 KHz [39]. The values of the parameters c_0^2 , c_2^2 and R_{\parallel} are given in Figure 8 of Reference [39].

there is no abrupt change in the diffusion rate-constants [39]. This is interpreted as follows: The amyloid-A β 40 fibrils exhibit several different water pools [103]. The bulk water freezes between 258 and 274 K [103]. Water freezing is transmitted to the fibril structure *selectively* through interactions with tightly-peptide-bound water. By virtue of its location at the fibril interface, the M35 methyl moiety is involved in such interactions. Our results indicate that tightly-peptide-bound water resides at both the inner and outer fibril interface. As pointed out above, the molecular environment responds in a specific manner to bulk-water-freezing: c_0^2 , c_2^2 and β_{MQ} do change abruptly when this occurs, whereas R_{\parallel} and R_{\perp} do not [39].

MOMD applied to deuterated phenyl-ring dynamics in amyloid-A β 40 fibrils. Our last example refers to the very same A β 40-amyloid fibrils investigated with MOMD using the deuterated phenyl ring of residue F19 as a probe [40]. The experimental ^2H spectra were taken from Reference [104], where MSM analysis was applied. To compare proteins in fibril and globular form, we also studied phenyl-ring motion in HP36; experimental ^2H spectra from the deuterated phenyl rings of F51 and F58 were taken from Reference [105]. All of the experimental lineshapes can be reproduced with comparable accuracy with an MSM model [105] and with MOMD [40]. However, several aspects of the MSM model used are problematic. Thus, the activation energy for one of the simple conformational-exchange modes is taken as an overall ordering potential. Moreover, the rate of this mode is slower than the rate of another mode which mixes the exchanging sites (cf. Reference [40]).

MOMD interprets restricted phenyl-ring dynamics in terms a local potential, $u = -c_0^2 D_{00}^2 - c_2^2 (D_{02}^2 + D_{0-2}^2)$, and an axial local diffusion tensor; best-fit β_{MQ} has standard value [40]. This consistent interpretation made possible comparing corresponding phenyl-ring sites in dry and hydrated fibrils; in the A β 40 fibrils and the protofibrils of the D23N-mutant; and in 2-fold-symmetric and 3-fold-symmetric A β 40 fibrils. Globular and fibril-type protein forms have also been compared. The local ordering played a key role in this study, as the form of the potential, u , was found to be the most sensitive feature in the analysis. Details appear in Reference [40].

Future prospects

The MSM fits might be termed ‘excellent’ whereas the MOMD fits are only ‘very good.’ But the MOMD parameter fitting has yet to be optimised to improve the agreement with the experiment. We have not done so at this stage. Instead, we explored the power of

MOMD when allowing the local ordering to be rhombic rather than axial, and the local diffusion to be axially symmetric rather than spherically symmetric. As seen above, model consistency made possible comparing various different systems labelled with the same probe. Improving the agreement with experiment will be pursued in the future work, in particular by using more detailed forms of the local ordering potential, as this has a large influence on the analysis. Work along these lines is in progress.

In this context, we recall that for ESR and NMR probes attached physically to the protein odd- L real linear combinations of Wigner rotation matrix elements, $D_{0|K|}^L$, should be included in the expression of the local potential. In Reference [106] using SRLS we analysed ^{15}N relaxation data from GB3 with both the $u = -c_0^2 D_{00}^2 - c_2^2 (D_{02}^2 + D_{0-2}^2)$ potential and the $u = -c_0^1 D_{00}^1 - c_1^1 (D_{0-1}^1 - D_{01}^1)$ potential. Order parameters S_0^2 and S_2^2 for the $L = 2$ potential, and S_0^1 and S_1^1 for the $L = 1$ potential, were determined. The two sets differed substantially in the β_1/β_2 loop, associated with GB3 binding to its cognate Fab fragment. In general, the application of SRLS to proteins utilising more detailed ordering potentials, which also include odd- L and/or higher L and K terms, and establishing a correlation between these potentials and biological function, are interesting future prospects.

MOMD analysis of ^2H spectra from polycrystalline proteins acquired in the presence of Magic Angle Spinning was developed in Reference [38]. Currently there are few experimental spectra suitable for such analysis. Work on the development of methodologies for acquiring spectra free of imperfections is ongoing [107]. Given that MAS substantially increases spectral sensitivity, the development of Reference [38] is likely to be very useful in the foreseeable future.

Conclusions

Molecular reorientation in the presence of spatial restraints has been considered from a rigid particle in a nematic solvent to a spin label in the interior space of a protein, with the protein tumbling in solution. Using well-developed theoretical approaches, we examined the concept of local ordering. We believe this has shown that insightful information can best be obtained using well-conceived dynamic models which enable consideration of the range of possibilities consistent with the experimental ESR and NMR spectra. The SLC, MOMD and SRLS models are useful approaches for treating restricted motions,

particularly in the slow-motional regime. The advantages inherent in oriented samples, 2D-ELDOR experiments, and multifrequency ESR for gaining insights into the characteristics of local ordering have been demonstrated. It was shown that macroscopically disordered samples can also provide valuable information. Currently, SRLS and MOMD are the methods of choice for characterising local ordering in proteins by ESR and NMR from a mesoscopic perspective, both in solution and in the solid-state.

Acknowledgments

It is with great sadness that we acknowledge the passing away of Prof. Zeev Luz of the Weizmann Institute, Rehovot, Israel. Zeev Luz made significant contributions to the study of the dynamic structure of molecules in anisotropic media by NMR and ESR. He pioneered, and uniquely promoted, the application of ^2H NMR to liquid crystals. His death deprives us of a highly esteemed scientist and much-valued mentor, teacher and friend. The entire Magnetic Resonance community mourns his loss.

Disclosure statement

No potential conflict of interest was reported by the authors.

Funding

This work was supported by the NIH under Grants P41GM103521 and R01GM123779 to J.H.F.; the ISF under Grant 369/15 to E.M.; and the BSF under Grant 2016097 to E.M. and J.H.F.; the National Institutes of Health [P41GM103521, R01GM123779]; Israel Science Foundation [369/15, Israel-USA Binational Science Foundation]; United States- Israel Binational Science Foundation [2016097].

ORCID

Eva Meirovitch  <http://orcid.org/0000-0001-5117-5079>
Jack H. Freed  <http://orcid.org/0000-0003-4288-2585>

References

- [1] de Gennes PG, Prost J. The physics of liquid crystals. Oxford, UK: Oxford University Press; 1993.
- [2] Jw E, Ed. NMR of liquid crystals. Dordrecht: Reidel; 1983.
- [3] Luckhurst GR, Veracini CA, Eds. The molecular dynamics of liquid crystals. The Netherlands: Kluwer Academic Publishers; 1994.
- [4] Collings PJ, Hird M. Introduction to liquid crystals: chemistry and physics. Boca Raton (FL): CRC Press; 1997.
- [5] Schenning A, Crawford GP, Broer DJ. Liquid crystal sensors. Boca Raton (FL): CRC Press; 2017.
- [6] Freed JH, Nayeem A, Rananavare S. ESR studies of molecular dynamics at phase transitions in liquid crystals. In: Luckhurst GR, Veracini CA, editors. 'The molecular dynamics of liquid crystals'. Vol. Chapter 14. Dordrecht, Netherlands: Kluwer; 1994. p. 335–364.
- [7] Liang Z, Freed JH. An assessment of the applicability of multifrequency ESR to study the complex dynamics of biomolecules. J Phys Chem B. 1999; 103:6384–6396.
- [8] Meirovitch E, Liang Z, Freed JH. Protein dynamics in the solid state from ^2H NMR lineshape analysis: a consistent perspective. J Phys Chem B. 2015;119:2857–2868.
- [9] Vold RL, Hoatson GL. Effects of jump dynamics on solid state nuclear magnetic resonance line shapes and spin relaxation times. J Magn Res. 2009;198:57–72.
- [10] Echodu D, Goobes G, Shajani Z, et al. Furanose dynamics in the *HhaI* methyltransferase target DNA studied by solution and solid-state NMR relaxation. J Phys Chem B. 2008;112:13934–13944.
- [11] Polnaszek CF, Bruno GV, Freed JH. ESR line shapes in the slow-motional region: anisotropic liquids. J Chem Phys. 1973;58:3185–3199.
- [12] Polnaszek CF, Freed JH. Electron spin resonance studies of anisotropic ordering, spin relaxation, and slow tumbling in liquid crystalline solvents. J Phys Chem. 1975;79:2283–2306.
- [13] Lin W-J, Freed JH. Electron spin resonance studies of anisotropic ordering, spin relaxation, and slow tumbling in liquid crystalline solvents. 3. Smectics. J Phys Chem. 1979;83:379–401.
- [14] Moro G, Freed JH. Calculation of ESR spectra and related fokker-planck forms by the use of the lanczos algorithm. J Chem Phys. 1981;74:3757–3773.
- [15] Moro G, Freed JH. Efficient computation of magnetic resonance spectra and related correlation functions from Stochastic Liouville Equations. J Phys Chem. 1980;84:2837–2840.
- [16] Meirovitch E, Ignier D, Ignier E, et al. Electron-Spin Relaxation and ordering in smectic and supercooled nematic liquid crystals. J Chem Phys. 1982;77:3915–3938.
- [17] Vasavada KV, Schneider DJ, Freed JH. Calculation of ESR spectra and related Fokker Planck forms by the use of the Lanczos algorithm. II. Criteria for truncation of basis sets and recursive steps utilizing conjugate gradients. J Chem Phys. 1987;86:647–661.
- [18] Budil DE, Lee S, Saxena S, et al. Nonlinear least-squares analysis of slow-motional ESR spectra in one and two dimensions using a modified Levenberg-Marquardt algorithm. J Magn Reson A. 1996;120:155–189.
- [19] Freed JH, Nayeem A, Rananavare S. ESR and liquid crystals: statistical mechanics and generalized Smoluchowski equations. In: Luckhurst GR, Veracini CA, editors. 'The molecular dynamics of liquid crystals'. Vol. Chapter 4. Dordrecht, Netherlands: Kluwer; 1994. p. 71–84.
- [20] Freed JH, Nayeem A, Rananavare S. ESR and molecular motions in liquid crystals: motional narrowing. In: Luckhurst GR, Veracini CA, editors. 'The molecular dynamics of liquid crystals'. Vol. Chapter 12. Dordrecht, Netherlands: Kluwer; 1994. p. 271–312.
- [21] Freed JH, Nayeem A, Rananavare S. Thermodynamics of liquid crystals and the relation to molecular dynamics: ESR studies. In: Luckhurst GR, Veracini CA, editors. 'The molecular dynamics of liquid crystals'. Vol. Chapter 13. Dordrecht, Netherlands: Kluwer; 1994. p. 313–333.

- [22] Freed JH, Nayeem A, Rananavare S. ESR and slow motions in liquid crystals. In: Luckhurst GR, Veracini CA, editors. 'The molecular dynamics of liquid crystals'. Vol. Chapter 15. Dordrecht, Netherlands: Kluwer; 1994. p. 365–402.
- [23] Budil DE, Earle KA, Lynch WB, et al. Electron Paramagnetic Resonance at 1 millimeter wavelengths. In: Hoff AJ, editor. 'Advanced EPR: applications in biology and biochemistry'. Vol. Chapter 8. Amsterdam: Elsevier; 1989. p. 307–340.
- [24] Lynch B, Earle KA, Freed JH. A 1 millimeter-wave ESR spectrometer. *Rev Sci Instrum.* 1988;59:1345–1351.
- [25] Patyal BR, Crepeau RH, Gamliel D, et al. Two-dimensional Fourier transform ESR in the slow-motional and rigid limits: 2D-ELDOR. *Chem Phys Lett.* 1990;175:453–460.
- [26] Gorcester J, Freed JH. Two dimensional fourier transform ESR spectroscopy. *J Chem Phys.* 1986;85:5375–5377.
- [27] Gorcester J, Freed JH. Two dimensional fourier transform ESR correlation spectroscopy. *J Chem Phys.* 1988;88:4678–4693.
- [28] Crepeau RH, Saxena S, Lee B, et al. Studies of lipid membranes by two-dimensional Fourier transform ESR: enhancement of resolution to ordering and dynamics. *Biophys J.* 1994;66:1489–1504.
- [29] Schneider DJ, Freed JH. Spin relaxation and molecular dynamics. *Adv Chem Phys.* 1989;73:387–528.
- [30] Meirovitch E, Nayeem A, Freed JH. Analysis of protein-lipid interactions based on model simulations of electron spin resonance spectra. *J Phys Chem.* 1984;88:3454–3465.
- [31] Patyal BR, Crepeau RH, Freed JH. Lipid-gramicidin interactions using two-dimensional fourier transform electron spin resonance. *Biophys J.* 1997;73:2201–2220.
- [32] Costa-Filho AJ, Crepeau RH, Borbat PP, et al. Lipid-gramicidin interactions: dynamic structure of the boundary lipid by 2D-ELDOR. *Biophys J.* 2003;84:3364–3378.
- [33] Ge M, Gidwani A, Brown HA, et al. Ordered and disordered phases coexist in plasma membrane vesicles of RBL-2H3 mast cells. *Biophys J.* 2003;85:1278–1288.
- [34] Cooper RS, Georgieva ER, Borbat PP, et al. Structural basis for membrane anchoring and fusion regulation of the herpes simplex virus fusogen gB. *Nat Struct Mol Biol.* 2018;2:416–424.
- [35] Lou Y, Ge M, Freed JH. A multifrequency ESR study of the complex dynamics of membranes. *J Phys Chem B.* 2001;105:11053–11056.
- [36] Liang Z, Lou Y, Freed JH, et al. A multifrequency Electron Spin Resonance study of T4 Lysozyme dynamics using the slowly relaxing local structure model. *J Phys Chem B.* 2004;108:17649–17659.
- [37] Meirovitch E, Liang Z, Freed JH. Protein dynamics in the solid state from ^2H NMR lineshape analysis. II MOMD applied to C–D and C–CD₃ probes. *J Phys Chem B.* 2015;119:14022–14032.
- [38] Meirovitch E, Liang Z, Freed JH. Protein dynamics in the solid-state from ^2H NMR lineshape analysis. III. MOMD in the presence of magic angle spinning. *Solid State Nucl Magn Reson.* 2018;89:35–44.
- [39] Meirovitch E, Liang Z, Freed JH. MOMD analysis of NMR lineshapes from A β -amyloid fibrils: a new tool for characterizing molecular environments in protein aggregates. *J Phys Chem B.* 2018;122:4793–4801.
- [40] Meirovitch E, Liang Z, Freed JH. Phenyl-ring dynamics in amyloid fibrils and proteins: the microscopic-order-macroscopic-disorder perspective. *J Phys Chem B.* 2018;122:8675–8684.
- [41] Polimeno A, Freed JH. A many-body stochastic approach to rotational motions in liquids. *Adv Chem Phys.* 1993;83:89–204.
- [42] Polimeno A, Freed JH. Slow-motional ESR in complex fluids: the slowly relaxing local structure model of solvent cage effects. *J Phys Chem.* 1995;99:10995–11006.
- [43] Zhang Z, Fleissner MR, Tipikin DS, et al. Multifrequency electron spin resonance study of the dynamics of spin-labeled T4 lysozyme. *J Phys Chem B.* 2010;114:5503–5521.
- [44] Liang Z, Freed JH, Keyes RS, et al. An electron spin resonance study of DNA dynamics using the slowly relaxing local structure model. *J Phys Chem B.* 2000;104:5372–5381.
- [45] Tugarinov V, Liang Z, Shapiro YE, et al. A structural mode-coupling approach to ^{15}N NMR relaxation in proteins. *J Am Chem Soc.* 2001;123:3055–3063.
- [46] Meirovitch E, Shapiro YE, Polimeno A, et al. Protein dynamics from NMR: the SRLS analysis compared with MF analysis. *J Phys Chem A.* 2006;110:8366–8396.
- [47] Meirovitch E, Shapiro YE, Polimeno A, et al. Structural dynamics of biomolecules by NMR: the slowly relaxing local structure approach. *Prog NMR Spectrosc.* 2010;56:360–405.
- [48] Meirovitch E, Polimeno A, Freed JH. Protein dynamics by NMR spin relaxation: the slowly relaxing local structure perspective. In: Harris RK, Wasylishen RE, editors. 'Encyclopedia of magnetic resonance'. U. K: John Wiley, Chichester; 2011. p. 3591.
- [49] Sastry VSS, Polimeno A, Crepeau RH, et al. Studies of spin relaxation and molecular dynamics in liquid crystals by two-dimensional Fourier transform electron spin resonance. I. Cholestane in butoxy benzylidene-octylaniline and dynamic cage effects. *J Chem Phys.* 1996;105:5753–5772.
- [50] Sastry VSS, Polimeno A, Crepeau RH, et al. Studies of spin relaxation and molecular dynamics in liquid crystals by two dimensional fourier transform ESR: II PD-tempone in butoxy benzylidene-octylaniline and dynamic cage effects. *J Chem Phys.* 1996;105:5773–5791.
- [51] Freed JH. Stochastic-molecular theory of spin-relaxation for liquid crystals. *J Chem Phys.* 1977;66:4183–4199.
- [52] Tchaicheyan O, Freed JH, Meirovitch E. Local ordering at mobile sites in proteins from nuclear magnetic resonance relaxation: the role of site symmetry. *J Phys Chem B.* 2016;122:886–2898.
- [53] *e-Chemical portal, D_{2h} point group.* <http://www.webqc.org/printable-symmetrypointgroup-d2h.html>
- [54] Zare RN. Angular Momentum. Vols. Ch. 5, Application 13. Hoboken (NJ): Wiley; 1988. p. 226.
- [55] Barnes JP, Freed JH. Dynamics and ordering in mixed model membranes of di-myristoyl-phosphatidylcholine and di-myristoyl-phosphatidyl-serine: a 250 GHz electron spin resonance study using cholestane. *Biophys J.* 1998;75:2532–2546.
- [56] Lipari G, Szabo A. Model-free approach to the interpretation of nuclear magnetic resonance relaxation in

- macromolecules. 1. Theory and range of validity. *J Am Chem Soc.* **1982**;104:4546–4559.
- [57] Clore GM, Szabo A, Bax A, et al. Deviations from the simple two-parameter Model-free approach to the interpretation of nitrogen-15 nuclear magnetic relaxation of proteins. *J Am Chem Soc.* **1990**;112:4989–4991.
- [58] Wand JA. The dark energy of proteins comes to light: conformational entropy and its role in protein function revealed by NMR relaxation. *Curr Opin Struct Biol.* **2013**;23:75–81.
- [59] Misra SK, Freed JH. Molecular motions. In: Misra SK, editor. *Multifrequency Electron Paramagnetic Resonance*. Vol. 11. New-York: Wiley-VCH; **2011**. p. 497–544.
- [60] Meirovitch E, Freed JH. Electron Spin Resonance studies of anisotropic ordering, spin relaxation, and slow tumbling in liquid crystalline solvents. 4. Cholestane motions and surface anchoring in smectics. *J Phys Chem.* **1980**;84:2459–2472.
- [61] Meirovitch E, Freed JH. Analysis of slow-motional electron spin resonance spectra in smectic phases in terms of molecular configuration, intermolecular interactions, and dynamics. *J Phys Chem.* **1984**;88:4995–5004.
- [62] Meirovitch E, Freed JH. ESR studies of low water content 1,2-dipalmitoyl-sn-glycero-3-phosphocholine in oriented multilayers. 1. Evidence for long-range cooperative chain distortions. *J Phys Chem.* **1980**;84:3281–3295.
- [63] Kar L, Ney-Igner E, Freed JH. Electron Spin Resonance and electron-spin-echo study of oriented multilayers of α -dipalmitoylphosphatidylcholine water systems. *Biophys J.* **1985**;48:569–595.
- [64] Tanaka H, Freed JH. Electron Spin Resonance studies on ordering and rotational diffusion in oriented phosphatidylcholine multilayers: evidence for a new chain-ordering transition. *J Phys Chem.* **1984**;88:6633–6644.
- [65] Tanaka H, Freed JH. Electron spin resonance studies of lipid-gramicidin interactions utilizing oriented multibilayers. *J Phys Chem.* **1985**;89:350–360.
- [66] Ge M, Freed JH. An electron spin resonance study of interactions between gramicidin A and phosphatidylcholine bilayers. *Biophys J.* **1993**;65:2106–2123.
- [67] Ge M, Budil DE, Freed JH. An electron spin resonance study of interactions between phosphatidylcholine and phosphatidylserine in oriented membranes. *Biophys J.* **1994**;66:1515–1521.
- [68] Shin YK, Mościcki JK, Freed JH. Dynamics of phospholipid membranes in liquid crystalline state. *Biophys J.* **1990**;57:445–459.
- [69] Shin YK, Mościcki JK, Freed JH. Dynamics of phosphatidylcholine-cholesterol mixed model membranes in the liquid crystalline state. *Biophys J.* **1990**;57:445–459.
- [70] Ge M, Freed JH. Electron-spin resonance study of aggregation of gramicidin in dipalmitoylphosphatidylcholine bilayers and hydrophobic mismatch. *Biophys J.* **1999**;76:264–280.
- [71] Costa-Filho A, Shimoyama Y, Freed JH. A 2D-ELDOR study of the liquid ordered phased in multilamellar vesicle membranes. *Biohy J.* **2003**;84:2619–2633.
- [72] Chiang Y-W, Costa-Filho A, Freed JH. Two-dimensional electron spin resonance study of model and biological membranes. *Appl Magn Res.* **2007**;31:375–386.
- [73] Borbat PP, Costa-Filho A, Earle KA, et al. Electron spin resonance studies of membranes and proteins. *Science.* **2001**;291:266–269.
- [74] Swamy MJ, Ciani L, Ge M, et al. Coexisting domains in the plasma membrane of live cells characterized by electron spin resonance spectroscopy. *Biophys J.* **2006**;90:4452–4465.
- [75] Ge M, Gidwani HA, Brown HA, et al. Ordered and disordered phases coexist in plasma membrane vesicles of RBL-2H3 mast cells. *An ESR Study Biophys J.* **2003**;85:1278–1288.
- [76] Ge M, Freed JH. Fusion peptide from hemagglutinin increases membrane surface order: as electron spin resonance study. *Biophys J.* **2009**;96:4925–4934.
- [77] Shorn K, Marsh D. Extracting order parameters from powder EPR lineshapes for spin-labeled lipids in membranes. *Spectrochim Acta A.* **1997**;53:2235–2240.
- [78] Marsh D. Spin-label order parameter calibrations for slow motion. *Appl Magn Reson.* **2018**;49:99–106.
- [79] Dzikovski B, Freed JH. Membrane fluidity. In: Roberts GCK, editor. *‘Encyclopedia of Biophysics’*. Vol. 425. Berlin, Germany: Springer Verlag; **2013**. p. 1440–1446.
- [80] Ge M, Freed JH. Polarity profiles in oriented and dispersed phosphatidylcholine bilayers are different: an electron spin resonance study. *Biophys J.* **1988**;74:910–917.
- [81] Ge M, Freed JH. Fusion peptide from influenza hemagglutinin increases membrane surface order: an electron-spin resonance study. *Biophys J.* **2009**;96:4925–4934.
- [82] Lai AL, Freed JH. The interaction between influenza HA fusion peptide and transmembrane domain affects membrane structure. A.L. Lai and J.H. Freed. *Biophys J.* **2015**;109:2523–2536.
- [83] Pinello JF, Lai AL, Millet JK, et al. Structure-function studies link class II viral fusogens and the ancestral gamete fusion protein HAP2. *Curr Biol.* **2017**;27:651–660.
- [84] Chiang YW, Costa-Filho AJ, Baird B, et al. 2D-ELDOR study of heterogeneity and domain structure changes in plasma membrane vesicles upon cross-linking of receptors. *J Phys Chem B.* **2011**;115:10462–10469.
- [85] Chiang Y-W, Costa-Filho A, Freed JH. 2D-ELDOR using full S_c fitting and absorption lineshapes. *J Magn Reson.* **2007**;188:231–245.
- [86] Mchaourab HS, Lietzow MA, Hideg K, et al. Motion of spin-labeled side chain in T4 Lysozyme. Correlation with protein structure and dynamics. *Biochemistry.* **1996**;35:7692–7704.
- [87] Barnes JP, Liang Z, Mchaourab HS, et al. A multifrequency electron spin resonance study of T4 Lysozyme Dynamics. *Biophys J.* **1999**;76:3298–3306.
- [88] Jarymowycz VA, Stone MJ. Fast time scale dynamics of protein backbones: NMR relaxation methods, applications, and functional consequences. *Chem Rev.* **2006**;106:1624–1671.
- [89] Kay LE, Torchia DA, Bax A. Backbone dynamics of proteins as studied by nitrogen-15 inverse detected heteronuclear NMR spectroscopy: application to staphylococcal nuclease. *Biochemistry.* **1989**;28:8972–8979.
- [90] Muhandiram DR, Yamazaki T, Sykes BD, et al. Measurement of ^2H T_1 and $T_{1,\text{rho}}$ relaxation times in

- uniformly ^{13}C -labeled and fractionally ^2H -labeled proteins in solution. *J Am Chem Soc.* **1995**;117:11536–11544.
- [91] Hall JB, Fushman D. Variability of the ^{15}N chemical shielding tensors in the B3 domain of protein G from ^{15}N relaxation measurements at several fields. Implications for backbone order parameters. *J Am Chem Soc.* **2006**;128:7855–7870.
- [92] Shapiro YE, Meirovitch E. Slowly relaxing local structure (SRLS) analysis of ^{15}N -H relaxation from the prototypical small proteins GB1 and GB3. *J Phys Chem B.* **2012**;116:4056–4068.
- [93] Meirovitch E, Shapiro YE, Tugarinov V, et al. Mode-Coupling analysis of ^{15}N CSA- ^{15}N - ^1H dipolar cross-correlation in proteins. Rhombic potentials at the N-H bond. *J Phys Chem B.* **2003**;107:9883–9897.
- [94] Lee AL, Sharp KA, Kranz JK, et al. Temperature dependence of the internal dynamics of a calmodulin-peptide complex. *Biochemistry.* **2002**;41:13814–13825.
- [95] Shapiro YE, Polimeno A, Freed JH, et al. Methyl dynamics of a Ca^{2+} -calmodulin-peptide complex from NMR/SRLS. *J Phys Chem B.* **2011**;115:354–365.
- [96] Lee AL, Wand AJ. Microscopic origins of entropy, heat capacity and glass transition in proteins. *Nature.* **2001**;411:501–504.
- [97] Sharp KA, Kasinath V, Wand AJ. Banding of NMR-derived methyl order parameters: implications for protein dynamics. *Proteins.* **2014**;82:21-6-2117. DOI:10.1021/prot.24566.
- [98] Tchaicheeyan O, Meirovitch E. An SRLS study of ^2H methyl-moiety relaxation and related conformational entropy in free and peptide-bound PLC $_{\gamma}$ 1C SH2. *J Phys Chem B.* **2016**;120:10695–10705.
- [99] Batchelder LS, Sullivan CE, Jelinski LW, et al. Characterization of leucine side-chain reorientation in collagen fibrils by solid-state ^2H NMR. *Proc Natl Acad Sci USA.* **1982**;79:386–389. PMID:6952191. PMCID: PMC345746
- [100] Wittebort RJ, Olejniczak ET, Griffin RG. Analysis of deuterium nuclear magnetic resonance line shapes in anisotropic media. *J Chem Phys.* **1987**;86:5411–5420.
- [101] Vugmeyster L, Ostrovsky D, Khadjinova A, et al. Slow motions in the hydrophobic core of chicken villin head-piece subdomain and their contributions to configurational entropy and heat capacity from solid-state deuterium NMR measurements. *Biochemistry.* **2011**;50:10637–10646.
- [102] Vugmeyster L, Clark MA, Falconer IB, et al. Flexibility and solvation of amyloid- β hydrophobic cores. *J Biol Chem.* **2016**;291:18484–18495.
- [103] Wang T, Jo H, DeGrado WF, et al. Water distribution, dynamics, and interactions with Alzheimer's β -amyloid fibrils investigated by solid-state NMR. *J Am Chem Soc.* **2017**;139:6242–6252.
- [104] Vugmeyster L, Ostrovsky D, Hoatson GL, et al. Solvent driven dynamical crossover in the phenylalanine side-chain from the hydrophobic core of amyloid fibrils detected by ^2H NMR relaxation. *J Phys Chem B.* **2017**;121:7267–7275.
- [105] Vugmeyster L, Ostrovsky D, Villafranca T, et al. Dynamics of hydrophobic core phenylalanine residues probed by solid-state deuterium NMR. *J Phys Chem B.* **2015**;119:14892–14904.
- [106] Tchaicheeyan O, Meirovitch E. Polar versus non-polar local ordering at mobile sites in proteins: slowly relaxing local structure analysis of ^{15}N relaxation in the third immunoglobulin-binding domain of streptococcal protein G. *J Phys Chem B.* **2016**;120:386–395.
- [107] Shi X, Rienstra CM. Site-specific internal motions in GB1 protein microcrystals revealed by 3D ^2H - ^{13}C - ^{13}C solid-state NMR spectroscopy. *J Am Chem Soc.* **2016**;138:4105–4119.